



**MODELING OF DRILLING OPERATION FOR SUPERALLOYS WITH
FINITE ELEMENT METHOD**

**A THESIS SUBMITTED TO
THE GRADUATE SCHOOL OF NATURAL AND APPLIED SCIENCES
OF
GAZI UNIVERSITY**

**BY
Mohammed Baqi Hussein HUSSEIN**

**IN PARTIAL FULFILLMENT OF THE REQUIREMENTS
FOR
THE DEGREE OF MASTER OF SCIENCE
IN
MECHANICAL ENGINEERING**

OCTOBER 2020

ETHICAL STATEMENT

I hereby declare that in this thesis study I prepared in accordance with thesis writing rules of Gazi University Graduate School of Natural and Applied Sciences;

- All data, information and documents presented in this thesis have been obtained within the scope of academic rules and ethical conduct,
 - All information, documents, assessments and results have been presented in accordance with scientific ethical conduct and moral rules,
 - All material used in this thesis that are not original to this work have been fully cited and referenced,
 - No change has been made in the data used,
 - The work presented in this thesis is original,
- or else, I admit all loss of rights to be incurred against me.

Mohammed Baqi Hussein HUSSEIN

04/10/2020

MODELING OF DRILLING OPERATION FOR SUPERALLOYS WITH FINITE
ELEMENT METHOD

(M. Sc. Thesis)

Mohammed Baqi HUSSEIN

GAZI UNIVERSITY

GRADUATE SCHOOL OF NATURAL AND APPLIED SCIENCES

October 2020

ABSTRACT

Finite element method has been used widely in metal cutting simulations in the last years. This method provides selecting the most advantageous cutting parameters for complex metal cutting operations, in terms of cost and time. In this thesis, drilling operation of aged Incoloy A286 superalloy, annealed and aged Inconel 718 superalloys were modeled numerically using Deform-3D V.11; and the effects of feed rate and cutting speed on thrust force and cutting torque were investigated. Two different feed rates and cutting speeds were used for drilling simulations for each material. In the drilling simulations of Incoloy A286, two twist drills with diameter 8.38 mm, helix angle 28 degree, point angles 120 degree and 140 degree found in the industry were scanned with 3D cameras and modelled again, then imported to the Deform-3D program. The twist drill used in the drilling simulations of Inconel 718 has a diameter of 5 mm, helix angle of 30 degrees and point angle of 140 degrees, which was modelled in the Deform-3D program. In the drilling simulations, Johnson-Cook material model was applied. Flow stress parameters of Incoloy A286, which were not available in the literature, were determined using quasi-static tensile tests at room temperature and Split-Hopkinson dynamic compression tests at room and high temperatures, while the parameters for Inconel 718 were obtained from the literature. The numerical results were agreed with the studies in the literature. The thrust force and torque were increased with the increase of feed rate and decreased with the increase of cutting speed within the studied cutting speed range.

Science Code : 91433, 91438
Key Words : Drilling, Inconel 718, Incoloy A286, FEM, Deform-3D
Page Number : 65
Supervisor : Dr. Lecturer. Yavuz ZUMRUT

SÜPER ALAŞIMLARA MATKAPLA DELİK DELME İŞLEMİNİN SONLU ELEMENLAR YÖNTEMİ İLE MODELLENMESİ

(Yüksek Lisans Tezi)

Mohammed Baqi Hussein HUSSEIN

GAZİ ÜNİVERSİTESİ
FEN BİLİMLERİ ENSTİTÜSÜ

Ekim 2020

ÖZET

Metal kesme işlemlerinin simülasyonunda sonlu elemanlar yöntemi son yıllarda oldukça yaygın olarak kullanılmaktadır. Yöntem, karmaşık metal kesme işlemlerinde işparçası ve istenilen çıktı parametreleri özellikleri doğrultusunda uygun kesici takım ve işlem parametrelerinin özellikle zaman ve maliyet bakımından oldukça avantajlı olarak belirlenmesine imkan vermektedir. Bu tezde, yaşlandırılmış Incoloy A286 süper alaşımı ile tavllanmış ve yaşlandırılmış Inconel 718 süper alaşımlarının matkapla delme işlemleri Deform-3D V.11 programı kullanılarak sayısal olarak modellenmiş; ilerleme ve kesme hızlarının itme kuvvetleri ve delme momentleri üzerine etkileri araştırılmıştır. Delme işlemi simülasyonları, her iki malzeme için de, iki farklı ilerleme hızı ve iki farklı kesme hızı değeri kullanılarak yapılmıştır. Incoloy A286 malzemesinin delinmesi için kullanılan matkap modelleri endüstride mevcut olan 8,38 mm çapında 120° ve 140°'lik uç açılarına ve 28°'lik helis açısına sahip iki farklı matkap ucunun taranması ile oluşturulmuş ve Deform programına aktarılmıştır. Inconel 718 malzemesi için kullanılan matkap modeli ise 5 mm çapında 140°'lik uç açısı ve 30°'lik helis açısına sahip olup Deform programının kendi içinde oluşturulmuştur. Simülasyonlarda, malzeme modeli olarak Johnson-Cook bünye denklemi uygulanmıştır. Incoloy A286 süper alaşımı için literatürde bulunamayan Johnson-Cook akma gerilmesi parametreleri, oda sıcaklığında yapılan çekme ve oda ile yüksek sıcaklıklarda yapılan Split-Hopkinson dinamik bası deneyleri ile belirlenmiş, Inconel 718 için ise literatürden alınmıştır. Elde edilen sayısal sonuçlar literatürdeki sonuçlar ile uyumludur. İtme kuvveti ve delme momenti artan ilerleme hızı ile artmakta, çalışılan kesme hızı aralığındaki artan kesme hızı ile azalmaktadır.

Bilim Kodu : 91433, 91438
Anahtar Kelimeler : Matkapla delik delme, Inconel 718, Incoloy A286, Sonlu elemanlar yöntemi, Deform 3D
Sayfa Adedi : 65
Danışman : Öğr. Gör. Dr. Yavuz ZÜMRÜT

ACKNOWLEDGEMENT

First and for most, I would like to express my sincere thanks to my supervisor Dr. Lecturer Yavuz ZÜMRÜT for his constant guidance, valuable support and advice throughout the writing process of this thesis. And I would like to thank Prof. Dr. Ahmet TAŞKESEN for his kind support and guidance. I also would like to thank my friends Bzhar and Govar for their support and help while preparing this study.

I would like to acknowledge the constant support and love provided by my family during all my education levels.

CONTENTS

	Page
ABSTRACT.....	iv
ÖZET	v
ACKNOWLEDGEMENT	vi
CONTENTS.....	vii
LIST OF TABLES	ix
LIST OF FIGURES	x
NOMENCLATURE	xiii
1. INTRODUCTION.....	1
2. DRILLING OPERATION	15
2.1. Metal Cutting Operations;.....	15
2.2. Drilling Operation	15
2.3. Cutting Conditions in Drilling	18
2.4. Cutting Forces and Power Consumption in Metal Drilling	19
2.5. Tool Wear.....	22
2.6. Cutting Temperature	24
3. MATERIAL AND METHOD	27
3.1. Material	27
3.1.1. Workpiece material and model.....	27
3.1.2. Drill geometry, material and model.....	28
3.1.3. Cutting conditions in the simulations	32
3.1.4. The Software program used for the numerical simulations.....	33
3.2. Method	33
3.3. Experimental Tests And Johnson-Cook Parameters Determination For Incoloy A286.....	34
3.3.1. Quasi–static tension tests.....	34

	Page
3.3.2. Dynamic tests	35
3.4. Background on Split Hopkinson Pressure Bar	35
3.4.1. A brief history about Split Hopkinson pressure bar	35
3.4.2. Split Hopkinson pressure bar apparatus	37
3.5. Quasi-Static Tensile Test Procedure	38
3.6. Dynamic Compression Test Procedure	41
3.7. Numerical Simulations	45
4. RESULTS AND DISCUSSION	49
4.1. Results	49
4.1.1. Simulation results	49
4.2. Discussion	50
5. CONCLUSION AND FUTURE WORK	55
5.1. Conclusion	55
5.2. Future Work	56
REFERENCES	57
ATTACHMENTS	61
Attachment-1. Incoloy A-286 Material Certificate	62
Attachment-2. International standard of material Incoloy A286	63
Attachment-3. Twist drill details used for drilling Incoloy A286	64
CURRICULUM VITAE	65

LIST OF TABLES

Table	Page
Table 1.1. Some typical superalloy compositions with strength properties	3
Table 1.2. Chemical composition of Incoloy A-286 Superalloy	5
Table 1.3. Typical physical properties of Incoloy A-286 Superalloy	5
Table 1.4. Limiting chemical composition of Inconel 718.....	9
Table 3.1. Chemical composition of Incoloy A-286 Superalloy.	27
Table 3.2. Twist drill mesh properties for Inconel 718.....	29
Table 3.3. Twist drill geometries and coating materials for Incoloy A286	29
Table 3.4. Simulation plan for drilling of aged and annealed Inconel 718.....	32
Table 3.5. Simulation plan for drilling of Incoloy A286	33
Table 3.6. Johnson-Cook model parameters for Inconel 718 [28]	34
Table 3.7. Room temperature (30 °C) and high temperature (270 °C) dynamic compression tests	42
Table 3.8. The J-C parameters determined for Incoloy A286	44
Table 3.9. Mesh details of workpieces for Inconel 718 and Incoloy A286 (above), Mesh details of drills for Incoloy A286 (below).	47
Table 3.10. Geometrical inputs and simulation parameters for Incoloy A286.....	47
Table 4.1. Simulation results for drilling Inconel 718	49
Table 4.2. Simulation results for drilling Incoloy A286.....	50

LIST OF FIGURES

Figure	Page
Figure 1.1. Tensile properties of age-hardened superalloy Incoloy A-286	6
Figure 1.2. Rupture strength of age-hardened superalloy Incoloy A-286	6
Figure 1.3. Creep strength of age-hardened superalloy Incoloy A-286.....	7
Figure 1.4. Material machinability.....	8
Figure 2.1. Drilling operation	15
Figure 2.2. Standard twist drill geometry	16
Figure 2.3. The material removal action along the cutting lips of a twist drill.....	17
Figure 2.4. Components of the drilling forces in drilling process.	19
Figure 2.5. Elements of undeformed chip in drilling.....	21
Figure 2.6. Factors affecting the drilling forces.....	22
Figure 2.7. Characteristic wear types and wear regions of a twist drill.....	23
Figure 2.8. The different wear types on the carbide drills.	24
Figure 3.1. Workpiece model cross-section.....	28
Figure 3.2. 5 mm diameter drill model	29
Figure 3.3. Twist drills designed in SolidWorks	30
Figure 3.4. AICON Smart Scan 3D system during scanning process	31
Figure 3.5. Twist drill with 120 degree point angle compared to scanned model.....	31
Figure 3.6. Twist drill with 140 degree point angle compared to scanned model.....	32
Figure 3.7. Typical dogbone specimen.	35
Figure 3.8. The Hopkinson experiment.	36
Figure 3.9. Davis experiment.....	36
Figure 3.10. The Kolsky bar	37
Figure 3.11. The schematic view of SHPB.....	38
Figure 3.12. Tensile test specimen, dimensions in (mm)	39

Figure	Page
Figure 3.13. The pictures of tensile test specimen mounted on tensile test machine before (at left) and after (at right) testing.....	39
Figure 3.14. Pictures of tested tensile test specimens	40
Figure 3.15. Engineering and true stress-strain curves for quasi-static tensile test.....	40
Figure 3.16. Cylindrical dynamic compression test specimen, dimensions in (mm)	41
Figure 3.17. Split Hopkinson pressure bar machine	41
Figure 3.18. Performing the high temperature dynamic compression test in Split Hopkinson pressure bar machine	42
Figure 3.19. Pictures of tested cylindrical specimens in dynamic compression tests.....	43
Figure 3.20. High strain rate dynamic compression tests at room temperature.....	43
Figure 3.21. High strain rate dynamic compression tests at room (30 °C) and high (270 °C) temperature.....	44
Figure 3.22. J-C curve fit for dynamic compression test at room temperature	45
Figure 3.23. J-C curve fit for dynamic compression test at high temperature.....	45
Figure 3.24. Johnson Cook model curve fitting in Deform 3D	46
Figure 4.1. Typical simulation results, steady state region and the mean value in Deform 3D	49
Figure 4.2. Increase of torques with increase of feed rate in drilling aged and annealed Inconel 718	50
Figure 4.3. Increase of thrust forces with increase of feed rate in drilling aged and annealed Inconel 718	51
Figure 4.4. Increase of torques with increase of feed rate in drilling Incoloy A286	51
Figure 4.5. Increase of thrust forces with increase of feed rate in drilling Incoloy A286.....	52
Figure 4.6. Decrease of torques with increase of cutting speed in drilling aged and annealed Inconel 718	52
Figure 4.7. Decrease of thrust forces with increase of cutting speed in drilling aged and annealed Inconel 718.....	53
Figure 4.8. Decrease of torques with increase of cutting speed in drilling Incoloy A286.....	53

Figure	Page
Figure 4.9. Decrease of thrust forces with increase of cutting speed in drilling Incoloy A286.....	54

NOMENCLATURE

Roman	Letter Symbols
A_c	Chip cross-sectional area, mm ²
b	Thickness of cut chip, mm
D	Diameter of the drill, mm
f	Feed, mm/rev
F_a	Thrust force, N
f_r	Feed rate, mm/min
F_r	Radial force, N
F_v	Circumferential force, N
h	Width of cut chip, mm
k_s	Specific cutting resistance, N/mm ²
l	Cutoff length, μ m
M	Drilling torque, Nmm
M_r	Drilling torque due to the radial force, Nmm
M_v	Drilling torque due to the circumferential force, Nmm
n	Number of deviations
N	Spindle speed, rev/min
N_c	Main drilling power, kW
N_{fd}	Feed power, kW
N_m	Motor power, kW
n_m	Mechanical efficiency of employed drilling machine
N_t	Total drilling power, kW
R_{MR}	Material removal rate, mm ³ /min
v	Cutting speed, m/min
w	Half of the web thickness, mm
y	Vertical deviations, μ m
Greek	Letter Symbols
β_o	Taper angle
k_t	Helix angle
χ	Lip angle

Acronyms	Letter Acronyms
3D	Three Dimensional
AOD	Argon Oxygen Decarburization
ASTM	American Society for testing and materials
DEFORM	Design Environment for Forming
BUE	Built-up Edge
FEM	Finite Element Method
CMM	Coordinate Measuring Machine
CNC	Computer Numerical Control
HRB	Hardness Rockwell measured on the B scale
HSS	High Speed Steel
HV	Hardness Vickers
J-C	Johnson-Cook
GW	Gradual Wear
LN2	Liquid Nitrogen
MQL	Minimum Quantity Lubrication
TiN	Titanium Nitrate
TiAlN	Titanium Aluminum Nitrate

1. INTRODUCTION

Metal cutting process has a great importance in manufacturing sector, because almost all industrial products are directly or indirectly exposed to the metal cutting processes during production, which mainly includes turning, milling, drilling, grinding, tapping, etc. Drilling is among the most important machining processes and used the most after turning and milling process [1], which occupies about 30% of metal cutting processes [2].

Generally the drilling process is a final metal cutting process. Drilling process is similar to turning and milling in dynamic and kinematic behavior, and the same in chip flow and heat distribution [3].

Investigating the right parameters for metal cutting operations experimentally, is time and money consuming. It is agreed that, it is possible to save this consumption up to 20% by selecting the right cutting parameters and right cutting tools for related machining operation [4]. Because of these reasons, researchers have spent a great effort on studying complex operations like drilling, numerically instead of traditional experimental ways, to save even more of the time and money consumption. Significant progress is seen in developing industry-driven predictive models for machining operations especially during the last few decades [5].

Finite element method (FEM) based software is involved in studying metal cutting operations widely. Especially for complex metal cutting operations of hard to cut metals and alloys, it is very advantageous in terms of time and cost to use these programs.

In drilling operation, the most important parameters which affect the yield of the drilling process and life of the tool, are the thrust force, torque, surface roughness, tool wear and burr formation. Choosing appropriate manufacturing conditions and the right cutting parameters, is necessary for a yielding drilling process. Therefore, many studies have been achieved on issues like cutting parameters, drill point angle and edge geometry. The goal of those studies are to minimize the thrust force, torque, tool and cutting zone temperature and burr formation for obtaining a desirable hole geometry, [6, 7, 8].

Superalloys

The superalloys are high-performance alloys designed to meet very inconvenient requirements for strength and resistance to surface corruptions at high temperatures. For these metals, usually traditional room temperature strength is not an important criterion, while most of the superalloys have room temperature strength properties which are good but not exclusive. What distinguishes them from other alloys, is their high temperature performance like; hot hardness, tensile strength, creep resistance, and corrosion resistance at very high temperatures. These alloys are widely used in gas turbines-jet and rocket engines, nuclear power plants-systems, and steam turbines where operating efficiency rises with higher temperatures [1].

The invention and improvement of superalloys were to provide better strength–weight ratio and higher heat and corrosion strength according to conventional alloys. Superalloys are preferred for offering better results especially in aerospace industry. They are generally used in manufacturing turbine and furnace pieces, oil refinery elements and chemical transportation equipment [9].

Typical superalloys contain high content of nickel, cobalt, iron, molybdenum, and chromium, in combination with up to fourteen elements. They are regarded as the most advanced alloys currently. The development and widespread applications of superalloys started with the development of gas turbine engines in the late of 1940s. Nowadays, they are preferred for aircrafts, power generation systems, nuclear reactors, chemical and petrochemical applications, medical devices, rocket engine components, cryogenic applications, etc. [10].

Usually the superalloys are categorized into three groups, according to their principal component like iron, nickel, or cobalt:

- Iron-based superalloys
- Nickel-based superalloys
- Cobalt-based superalloys

Iron based superalloys

They have iron as the main ingredient, although in some cases the iron is less than 50% of the total composition [1].

Iron-based superalloys are used in applications where high toughness and ductility are required. Turbine discs and forged rotors are two application examples for these superalloys. They are used only wrought condition to obtain desirable grain size and morphology. Owing to high Fe % content in their chemical composition, their cost is lower than the other superalloys [11].

Nickel based superalloys

These alloys have better temperature strength than alloy steels in general. As nickel is the base metal, the principal elements in these alloys are chromium and cobalt. They generally include lesser rates of titanium, aluminum, molybdenum, niobium and iron. The familiar types in this group of superalloy are, Inconel, Rene 41 and Hastelloy [1].

Cobalt based superalloys

Around 40% of the composition of these alloys is cobalt and 20% is chromium as their main components. This group also include other alloying elements like nickel, tungsten and molybdenum [1]. Some typical superalloy compositions with strength properties are shown in Table 1.1

Table 1.1. Some typical superalloy compositions with strength properties [1]

Superalloy	Chemical Analysis, % ^a							Tensile Strength at Room Temperature		Tensile Strength at 870°C (1600°F)	
	Fe	Ni	Co	Cr	Mo	W	Other ^b	MPa	lb/in ²	MPa	lb/in ²
Iron-based											
Incoloy 802	46	32		21			<2	690	100,000	195	28,000
Haynes 556	29	20	20	22	3		6	815	118,000	330	48,000
Nickel-based											
Incoloy 807	25	40	8	21		5	1	655	95,000	220	32,000
Inconel 718	18	53		19	3		6	1435	208,000	340	49,000
Rene 41		55	11	19	1		5	1420	206,000	620	90,000
Hastelloy S	1	67		16	15		1	845	130,000	340	50,000
Nimonic 75	3	76		20			<2	745	108,000	150	22,000
Cobalt-based											
Stellite 6B	3	3	53	30	2	5	4	1010	146,000	385	56,000
Haynes 188	3	22	39	22		14		960	139,000	420	61,000
L-605		10	53	20		15	2	1005	146,000	325	47,000

Superalloy Incoloy A-286

Incoloy A-286 superalloy is an iron-base superalloy and it is useful for applications requiring high strength and corrosion resistance up to 704°C and for lower stress applications at higher temperatures. Incoloy A-286 alloy is a heat and corrosion resistant austenitic iron-base material which can be age hardened to a high strength level. It is also used for low temperature applications requiring a ductile, non-magnetic high strength material at temperatures ranging from above room temperature down to at least -196°C. A-286 may be used for moderate corrosion applications in aqueous solutions. A-286 superalloy can be produced by AOD (Argon Oxygen Decarburization) refining or vacuum induction melting. Vacuum arc or electroslag remelting procedures may be used to further refine the material [12].

The high strength and excellent fabrication characteristics of superalloy A-286 make the alloy useful for various components of aircraft and industrial gas turbines. It is also used for fastener applications in automotive engine and manifold components subject to high levels of heat and stress and in the offshore oil and gas industry [13].

Some common industry applications of A-286 are;

- Jet engine components
- Fasteners
- Springs
- After Burner Parts
- Industrial Gas Turbines
- Moderate corrosion application in Aqueous Solutions
- Non-Magnetic Cryogenic Equipment.

Chemical composition and typical physical properties of Incoloy A-286 Superalloy are presented in Table 1.2 and Table 1.3 respectively.

Table 1.2. Chemical composition of Incoloy A-286 Superalloy [14]

ELEMENTS	PERCENTAGE %
C	0.05
Mn	1.00 - 2.00
Si	0.40 - 1.00
P	0.02 - 0.04
Ni	24.0 - 27.0
Mo	1.0 - 1.75
Ti	1.75 - 2.60
Cr	13.5 - 16.0
B	0.002- 0.015
V	0.10- 0.50
Al	0.16 - 0.36
S	0.01 - 0.02
Fe	Balance

Table 1.3. Typical physical properties of Incoloy A-286 Superalloy [14]:

Density	7.94 g/cm ³ at room temperature
Thermal Conductivity	0.05 Cal/cm ² /sec/cm/°C at 600 °C
Average Coefficient of Thermal Expansion	17.0 μm/cm/°C at 600°C
Specific Heat	0.11 Cal/cm ² °C (20-700°C)
Electrical Resistivity	91.0 microhm-cm at 30.6 °C

Critical temperatures of Incoloy A-286

Melting temperature range for Incoloy A-286 is between 1371 °C and 1426 °C, and intermetallic precipitation reaction temperature range is between 750 °C and 800 °C

Mechanical Properties of Incoloy A-286

In the age-hardened condition, superalloy Incoloy A-286 has high strength at room temperature and retains high levels of strength at temperatures to about 700°C [13]. Figure 1.1. shows the effect of temperature on tensile properties. Superalloy Incoloy A-286 has good creep-rupture strength during extended high-temperature exposure [13]. Figure 1.2. shows stresses for 100 and 1000 hour rupture lives at various temperatures. Stress levels to produce creep rates of 1%/100 h and 1%/1000 h are shown in Figure 1.3.

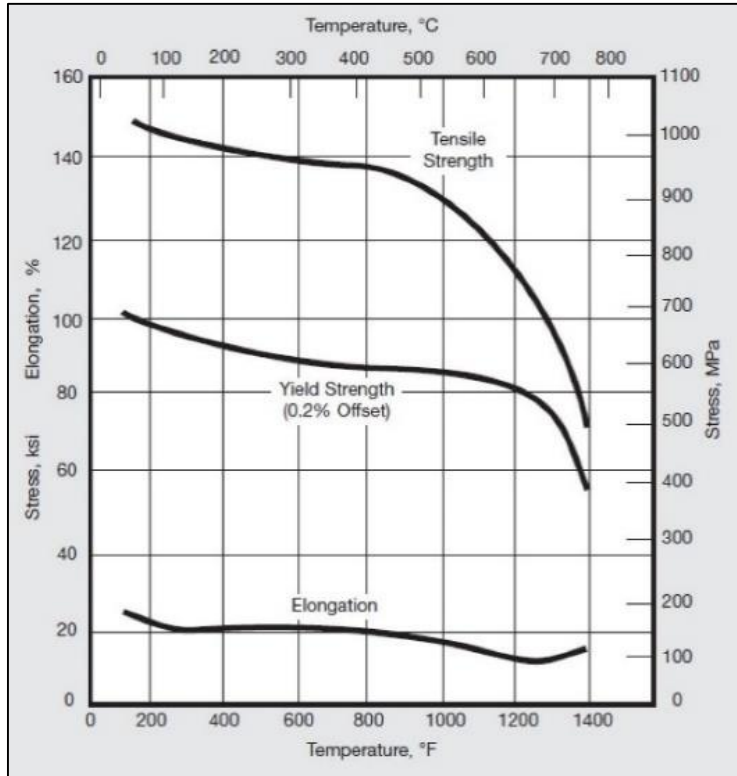


Figure 1.1. Tensile properties of age-hardened superalloy Incoloy A-286 [13]

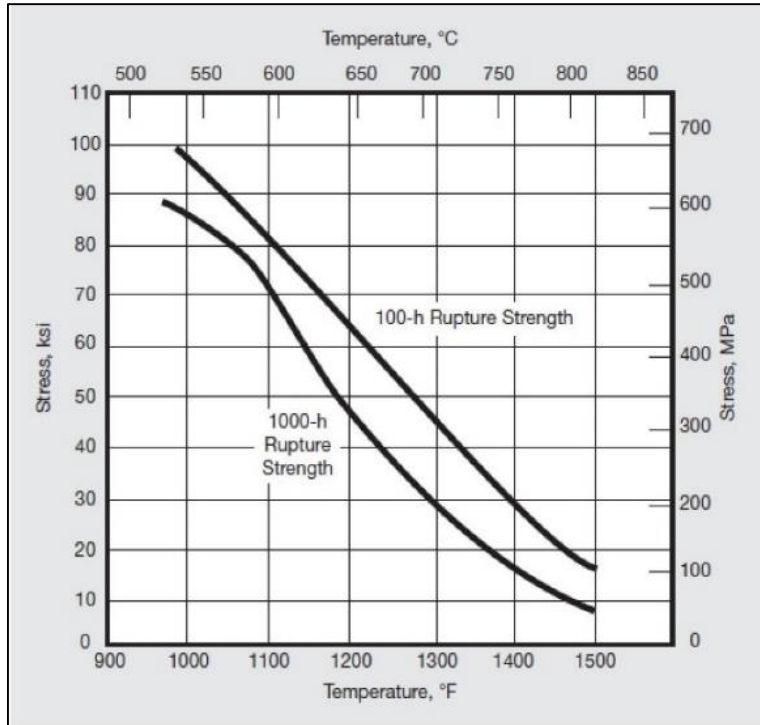


Figure 1.2. Rupture strength of age-hardened superalloy Incoloy A-286 [13]

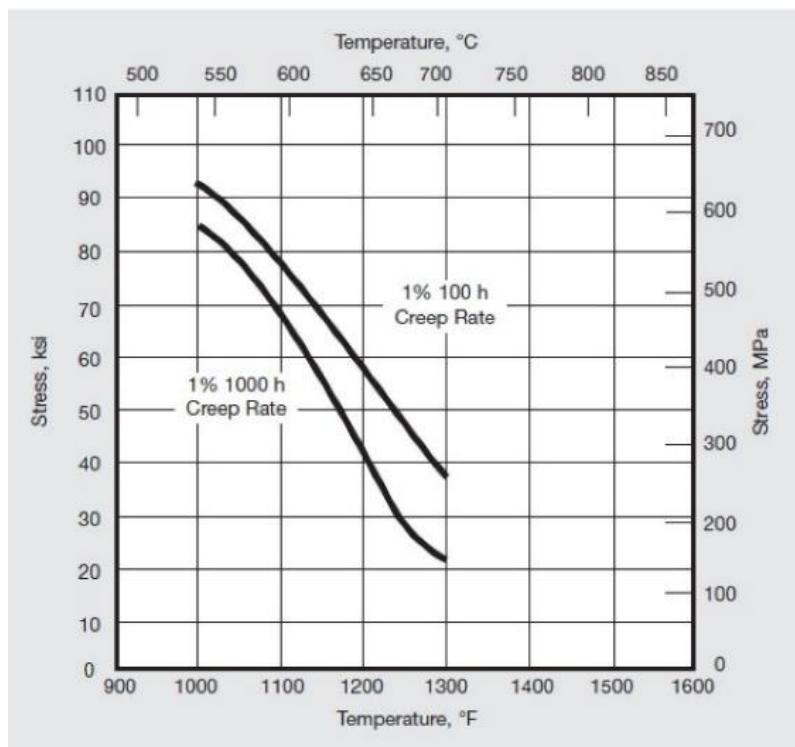


Figure 1.3. Creep strength of age-hardened superalloy Incoloy A-286 [13]

Mechanical properties reported here are for material given the following heat treatment: solution treatment at (980°C)/1h, cooling plus age hardening at (720°C)/16 h and air cooling.

Strengthening mechanisms for Incoloy A-286

Optimum properties of Incoloy A-286 are obtained by heat treating and aging (precipitation hardening). Thus, it is not necessary to work it in the temperature range of (538 to 816 °C) to produce high yield strengths as is required for other high-temperature alloys. (However, some properties are affected by cold working after aging, so that modified heat treatments may be required.) Solution treatment at 982 °C provides optimum stress-rupture properties after aging; solution treatment at 899°C provides maximum room temperature yield strength or short-time properties. After solution treating, Incoloy A-286 is soft (about 160 -170 HV) and is in its most ductile condition. Aging at (704° - 760°C) results in an increase of hardness to 275 - 300 HV. The high strength of the alloy is developed during the aging treatment by the random formation of a fine precipitate of [Ni₃ (Ti, Al)] in the austenitic matrix [14].

Joining Techniques of Incoloy A-286

In the group of precipitation-hardening austenitic stainless steels, Incoloy A-286 is the most weldable steel. It can be joined satisfactorily by fusion welding, resistance welding, and

brazing. Welding processes are similar to those used for welding austenitic stainless steels [14].

Machinability of Incoloy A-286

Incoloy A-286 superalloy, beside the high strength characteristics, has excellent fabrication characteristics. Incoloy A-286 superalloy is slower to machine than the 300 series of stainless steels, and exhibits the same gumminess and work hardening characteristics, so that rigid machine setup and sharp tools are required. To overcome the gumming condition, the superalloys is often partially aged (1 hour at 718 °C) or fully aged (16 hours at 718 °C), or over-aged (several hours at 716 °C) prior to machining. After over-aging and machining, re-solution treating and aging are required to develop optimum properties. Other suggestions for successful machining include the use of relatively low cutting speeds with recommended cutting fluids to reduce buildup edge, friction, and tool-chip temperatures. By using sharp tools of recommended geometries, work hardening is minimized. Also, tools should cut, not push, metal and they should never rub or dwell in the cut [14]. The Figure 1.4. shows the machinability comparison of Incoloy A-286 with other high strength superalloys and steels.

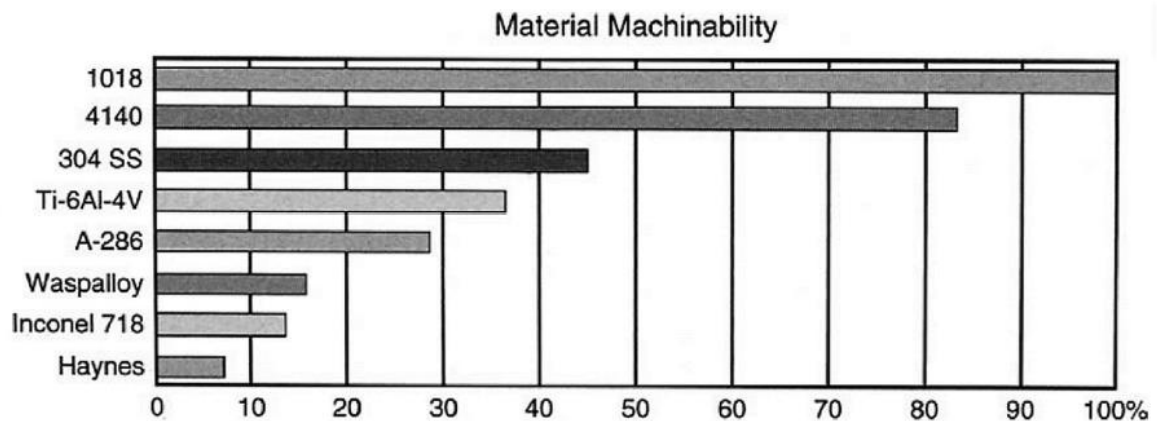


Figure 1.4. Material machinability [15]

Inconel 718

Inconel 718 is one of the most important nickel based superalloys. It is a high strength superalloy resistant to the variety of corrosive conditions, pitting and crevice corrossions. It provides superior mechanical properties like high tensile, fatigue and creep-rupture strength at high temperatures. It is also used at cryogenic (-252 °C) to high (704 °C) temperatures. Aeronautics and land based gas turbines, marine engineering, nuclear power plants, are the main fields of applications for this superalloy. [44, 45].

This nickel based superalloy is studied by researchers the most among the superalloys, due to its importance. Although there are less numerical simulations for metal cutting operations of Inconel 718 in the literature, many researchers have determined the Johnson-Cook constitutive model parameters for this alloy.

The limiting chemical composition of Inconel 718 is given in the Table 1.4.

Table 1.4. Limiting chemical composition of Inconel 718 [44]

ELEMENTS	Min %	Max %
Nickel + Cobalt	50.00	55.00
Chromium	17.00	21.00
Iron	Balanced	
Niobium + Tantalum	4.75	5.50
Molybdenum	2.80	3.30
Titanium	0.65	1.15
Aluminum	0.20	0.80
Cobalt	1.00
Carbon	0.08
Manganese	0.35
Silicon	0.35
Phosphorous	0.015
Sulfur	0.015
Boron	0.006
Copper	0.30

Literature Review

Metal cutting operations are still the most popular manufacturing techniques used in the industry. There are many studies in the literature performed for improving the product quality in metal cutting. Finding the right cutting parameters is the leading purpose of those studies. And the real purpose behind all of the studies, is to minimize the production cost and increase productivity. Most of the studies performed in the past are experimental studies, but it is time and money consuming to carry out the right cutting parameters, for each cutting operation and each type of materials and cutting tools experimentally. Because of this, numerical studies are involved too, especially for most complex metal cutting operations like drilling, and working on hard to cut materials like superalloys. Significant progress is seen in developing industry-driven predictive models for machining operations especially during the last few decades [5].

While reviewing the literature, many studies are found on drilling superalloys and low machinability materials experimentally, but less studies are done using simulations and numerical ways. So that in this thesis some of the experimental studies have been reviewed too. Also because studies are not available on drilling parameters of iron-based super alloy A-286, some of the studies have been reviewed too, which are performed on different superalloys and other materials so as to have an idea.

Uçak and his friends have analyzed numerically and experimentally the drilling operation on Inconel 718, to study thrust force, torque and drill temperature. They used Deform 2D and 3D to simulate the operation and observed a good agreement between the numerical and experimental results, [16].

Nicolas Beer and his friends, to increase the resistance against abrasive wear and to decrease the thermal loads; so that, to increase tool life and bore quality, tried geometry-modified tool in drilling of Inconel 718 superalloy. They used ANSYS/CFX to simulate the drilling operation and according to the study, the tool life and bore quality was improved using the new tool geometry [17].

A. Attanasio and his friends studied the simulation of tool wear in drilling nickel based super alloys. Based on experimental tool wear data, they used standard coated cemented carbide (TiAlN coating) twist drills to drill Inconel 718 in Deform 3D software. The Johnson-Cook constitutive model has been used in the numerical analysis and compared the results with the experimental data. From the comparison done, low errors between predicted and measured data was noticed, ranging from -3.3% to +9.6% demonstrating that the developed simulation procedure can correctly simulate the tool wear in drilling operation [18].

Using a 3D FEM simulation, Asit Kumar Parida has studied drilling operation of Ti-6Al-4V, to analyze thrust force, torque, stress, strain and drill bit temperature, by changing cutting speed and feed rates. Parida has compared the simulation results with experimental results and a close agreement with few errors was observed [19].

By varying the feed rate and cutting speed, Uçun studied the performances of twist drills and 3-flute drills while drilling Al7075-T6 alloy. Comparing the simulation results with experimental results, no significant error was observed. The author has also concluded that the twist drill performance was better than the 3-flute drill in drilling Al7075-T6 alloy. [11]

M. Nagaraj and his friends simulated drilling operation of Nimonic C-263 superalloy to study the thrust force, temperature generation, effective stress, and effective strain. They used Johnson–Cook (JC) material model to model the workpiece. They compared the obtained thrust force and drill bit temperature with the experimental results, and observed 10% of error [10].

Parvin Pawar and her friends simulated the drilling operation of Ti-6Al-4V and Al6061 materials using Deform 3D software and compared the results. They stated that, the Ti-6Al-4V alloy shows greater effective stress and temperature during the drilling process compared to the Al6061 material, which may possibly be because of physical properties of Ti-6Al-4V alloy [20].

A. Díaz-Álvarez and his friends studied experimental and numerical analysis of the influence of drill point angle when drilling bio-composites. They tested two types of twist drill bits (HSS and HSS customized) to drill a bio-degradable material (Flax as fibers and PLA) of different thicknesses. They used ABAQUS/Explicit for modeling the numerical analysis and imported drill bit models from CAD software. They tried six different point angles for the twist drills and compared thrust force, damage factor (F_d) at entry and exit of the drill for each drill point angle (118° , 110° , 100° , 90° , 80° and 70°), in seven different cases. They found out experimentally and numerically that increasing the point angle leads to increase thrust force in all cases. As the feed was increased, it was observed that the effect of the drill point angle was more significant. Result of the numerical analysis showed that choosing the point angle 70° , is the best option in terms of the thrust force and drilling induced damage [21].

Bagci, E. and Ozcelik, B. studied drilling steel AISI 1040 and Aluminum AL 7075-T651 experimentally and numerically using cooling fluids. In the study heat is predicted using FEM program (Third Wave Advantage). They have used uncoated, (TiN, TiAlN) coated carbide twist drills in dry and cooled drilling operations and placed thermocouples in the cooling fluid canals for recording the temperature [22].

Lin and her friends have modeled drilling operation and studied the effects of cutting speed and feed rate on the cutting forces and surface roughness. They have compared the simulation results with experimental results and discussed those effects [23].

J.S. Strenkowski et al, have developed an analytical finite element technique for predicting thrust force and torque in drilling AISI 1020 with twist drills using several spindle speeds and feed rates. The cutting forces along the cutting lips were represented as a series of oblique sections. Similarly, in the chisel region cutting was proceeded as orthogonal cutting with different cutting speeds based on the radial location. To simulate the cutting forces, an Eulerian finite element model was used for each section. A good agreement was found between the predicted and measured values of the forces and torques, [24].

Necati Uçak has experimentally studied the drillability of Inconel 718, under different cutting and cooling/lubrication conditions. The effects of cooling/lubricating conditions and coating material on drillability of Inconel 718 were evaluated. According to the results of the experiments, cryogenic drilling exhibited better performance on hole quality and surface integrity with less burr formation at the entrance and the exit of the hole, more accurate hole diameter, less roundness error, better machined subsurface quality, etc. However, it was determined that cryogenic conditions increased the thrust force and significantly reduced the tool life due to excessive chippings. Experiments under dry conditions did not show any superior performance to other conditions. Good surface roughness values and tool life were achieved in drilling test under wet conditions. It was also seen that, the increased cutting speed improved the cutting performance, especially in cryogenic conditions. The use of the coating material (TiAlN) also reduced the tool wear dramatically [25].

Kıvık, T. et al, experimentally investigated drilling Inconel 718 using coated and uncoated twist drills to study the effects of the cutting parameters on cutting forces. The experiments were performed with uncoated and (TiN, TiAlN) coated drills without using cooling fluids. According to the study, the best performance in terms of the cutting forces were observed when using the uncoated drills. Generally it was observed that, the feed rate was more effective on increasing the cutting forces, than the cutting speed [26].

Ali Rıza Motorcu and his friends experimentally studied the effects of feed rate, cutting speed, cutting tool type and drill bit point angle on the surface roughness in drilling operation of Waspaloy superalloy using coated and uncoated carbide drills. They used Minitab 16.0 package program for roughness, Ra measurement of the hole surface. According to the experimental and numerical results, most effective parameters on surface roughness (Ra) were determined as drill bit angle, feed rate, cutting speed and cutting tool type with 49,44%,

15,0%, 14,45% and 13,47% contribution ratios, respectively. And with the increasing of tool wear, surface roughness values increased [9].

Kemal Nazım Şekerci in his study has experimentally investigated the effect of different cutting parameters on cutting forces, torque, and surface roughness during drilling process. He has drilled austenitic type AISI 316L stainless steel with two different type of (uncoated and TiN/TiAl/TiCN coated solid carbide) HSS cutting tools. The experiments were performed by using fixed drill-rotating workpiece method. 32 experiments were performed using 16 coated and 16 uncoated drills. According to the experiment results, as feed rate increased, temperature in the cutting area was decreased. This decrease in temperature made chip flow easier and about 80% of the heat left the cutting area with the chip flow. As the cutting speed increased, temperature in the cutting area decreased and this decreasing was more significant in the experiments done with coated drills compared to the uncoated ones [27].

T. Ozel et al, made a comparison of 3D machining models using ABAQUS/Explicit and DEFORM 3D as two commercially available FE based software programs, for machining Inconel 718 superalloy. They compared the simulation results for temperature, strain and strain rate and stress distributions. They applied Johnson-Cook material model with Updated Lagrangian (DEFORM-3D) and ALE (ABAQUS/Explicit). According to the results of the study, predicted cutting forces were larger than experimental forces using the Johnson-Cook material model with both models [28].

K. Gok and his friends, studied simulation of AISI 1040 material. They used a 10 mm (HSS) drill bit with three different helix angles of 20, 25 and 30 degrees and a point angle of 118 degrees. By varying the feed rates, values of the thrust force and torque were obtained for each simulation. They compared the numerical results with experimental results and observed a good agreement between them [29].

Osman Bıyık experimentally tested Incoloy A-286 superalloy for dry drilling operation with carbide twist drills of point angles 120 degree and 140 degree having three different coating materials (TiN, TiAlN and AlCrN). The effects of cutting speed, feed rate, tool material and their interactions on drilling forces, torque and surface roughness were studied. Lower drilling forces were recorded when TiAlN coated drill with 120 degree point angle was used.

Cutting forces and surface roughnesses were increased with increasing the feed rate, while the increase in cutting speed decreased the surface roughness [30].

Aim of the thesis

The aim of this thesis is to model the drilling operation simulations on superalloys Incoloy A286 and Inconel 718 using Finite Element Based program Deform 3D. To do this, applying a deformation model is needed with determining the model parameters. The Johnson Cook (J-C) material model is applied. The J-C parameters for Inconel 718 is obtained from the literature, but model parameters for Incoloy A286 are not found in the literature. Therefore one of the main goals of this thesis is to determine the Johnson-Cook parameters for superalloy Incoloy A286 and to use in the simulations.

2. DRILLING OPERATION

2.1. Metal Cutting Operations;

In the industry, metal cutting processes are used for obtaining the final desired geometry of most mechanical parts. After a deformation process like casting, forging or rolling, by using one or more machining process types, the excess material is removed from the starting work part to obtain the desired shapes, dimensions, tolerances and surface quality. Turning, milling and drilling are the most popular machining processes [3].

2.2. Drilling Operation

Drilling operation is used for creating round holes, Figure 2.1. It is accomplished by a rotating tool that typically has two cutting edges. Generally the tool is fed in a direction parallel to the axis of rotation into the work piece, to create the round hole [1].

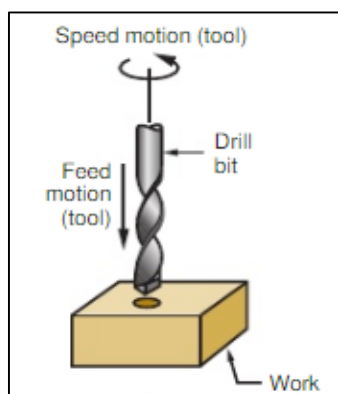


Figure 2.1. Drilling operation [1]

Drilling is one of the most important machining processes. Generally the drilling process is a final metal cutting process. Drilling process is similar to turning and milling in dynamic and kinematic behavior, and the same in chip flow and heat distribution [3].

Most drilling operations are performed using a rotating cylindrical tool with two cutting edges. The tool is called a drill or drill bit, and the most common type of which is the twist drill. The rotating drill bit feeds into the stationary work part to create a hole with a diameter equal to the diameter of the drill. Drilling is generally performed on a drill press, although other machine tools can perform this operation [1].

If the process is performed on a drilling machine, the workpiece is fixed and the drill bit turns and moves across its axis towards the workpiece, so the cutting operation takes place.

There are different cutting tools to perform hole making process, but twist drills are the most common type.

A twist drill has a chisel edge at the center and two or more helical cutting lips with a taper angle (K_t) that meet with the flutes with a helix angle (β_o).

Basically, a twist drill is composed of shank, drilling body and drill point. The shank is the part required to clamp the drill to the tool holder. Point of the drill is the part which cuts the workpiece and helps in conveying the chips out of the cutting zone through the flutes. The flutes, are located on the drill body, which have no contributions to cutting but have the responsibility to evacuate the chip to outside the hole and transfer the coolant to the cutting zone in case of using cooling fluids. The helix angle, as one of the most important factors regarding the flutes of the drill, affects the efficiency of drilling by influencing the rake angle distribution along cutting edges and chip evacuation time. Additionally, the most important parts in drill bit design are the drill point and the point angle, because the drilling process occurs at these [31]. A standard twist drill geometry is illustrated in the Figure 2.2.

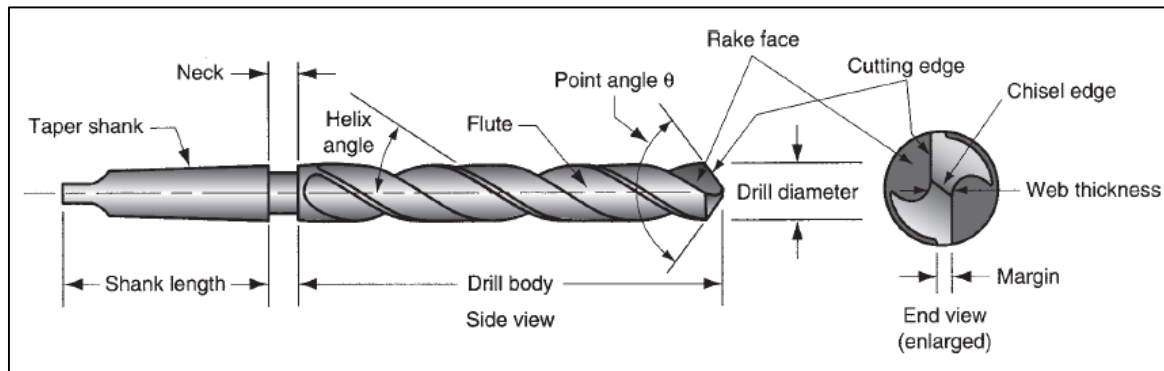


Figure 2.2. Standard twist drill geometry [1]

The cutting action in drilling process is complicated. The relative motion between cutting edges of the drill bit and the workpiece occurs with the rotational motion and the feed of the drill bit. Thus, chip formation takes place. The cutting speed changes along the cutting edges during drilling operation. Accordingly, maximum cutting speed occurs at the outer diameter of the drill and therefore, most effective cutting action occurs at these points.

Besides, at the drill point no cutting action takes place, because at the chisel edge relative velocity is zero. This part feeds into the workpiece material and thrusts aside the material at the center. To perform this motion, a great quantity of thrust force is needed. Because of that, at the beginning of the drilling operation, the thrust force value is higher during the penetration of the twist drill into the material. The material removal action along the cutting lips of a twist drill is illustrated in Figure 2.3.

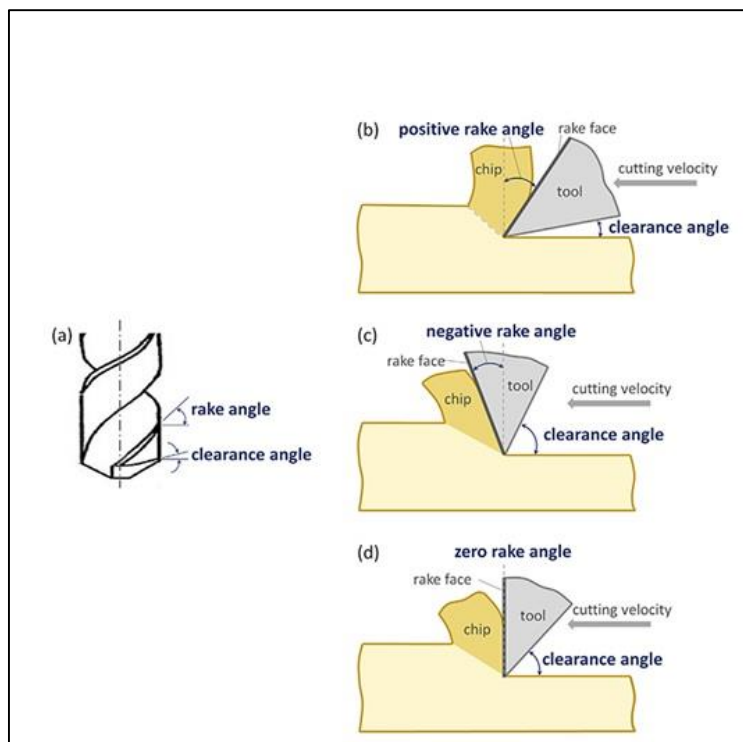


Figure 2.3. The material removal action along the cutting lips of a twist drill [32]

Because of the fact that cutting action takes place inside the hole in drilling operations, one of the serious problems is chip evacuation. The flutes of the drill must ensure adequate clearance along the length of the drill body to provide chip flow to outside the hole. When the chip forms by the motion of the drill, it is forced outward from the hole through the flutes. In metal cutting, the main friction occurs between the rake face of the drill bit and the chip. In addition to the main friction, secondary friction also occurs between the new machined surface and the outer surface of the drill due to rubbing motion. This leads to the increases in temperature in the cutting zone. The cutting fluids used in order to decrease friction and cutting temperatures cannot provide efficient cooling and lubrication requirements in drilling. Since the flow direction of the chips is opposite with the feed direction. This prevents the cutting fluids to reach the chisel edge as required.

This situation leads to limit the hole length in drilling operation [16]. In drilling operation, it is recommended that the hole depth in drilling operation should be three times the diameter of the drill at most [18]. If drilling depth exceeds, insufficient chip clearance, tool deflection, and failure problems can happen. Generally if deeper holes needed to be drilled, peck drilling method or custom designed drills should be used.

2.3. Cutting Conditions in Drilling

The cutting speed in a drilling operation is defined as the surface speed at the outside diameter of the drill. It is explained this way for convenience, otherwise most of the cutting is actually performed at lower speeds closer to the axis of rotation.

It is needed to determine the rotational speed of the drill for setting the desired cutting speed in drilling operation. The spindle speed N (rev/min), is calculated as follows;

$$N = \frac{V}{\pi D} \quad (2.1)$$

where V is cutting speed, mm/min; and D is the drill diameter, mm. When the workpiece is rotated about a stationary tool in some cases, the same formula is applied.

Feed f in drilling is described in mm/rev. The values of feed is directly proportional with the drill diameter. So greater feed values are in greater drills.

Since there are usually two cutting edges on a twist drill, uncut chip thickness (chip load) is equal to half of the feed.

Feed in drilling operation can be converted to feed rate using the same equation as for turning operation:

$$f_r = Nf \quad (2.2)$$

The material removal rate R_{MR} (mm³/min) in drilling is calculated as follows:

$$R_{MR} = \frac{\pi D^2 f_r}{4} \quad (2.3)$$

2.4. Cutting Forces and Power Consumption in Metal Drilling

The main components of the drilling forces on a twist drill are shown in Figure 2.4. The force components are positioned at a distance ($D/4$) from the drill center. Each component is subdivided into three components. Where, F_{a1} and F_{a2} represent the thrust force components which are parallel to the drill axis and in the same direction with feed. F_{v1} and F_{v2} are the circumferential (cutting) force components. They are perpendicular to the projection of cutting lips in the plane normal to the drill axis. Finally, F_{r1} and F_{r2} the radial force components, which are parallel to the projection of cutting lips in the plane normal to the drill axis.

The total axial drilling force , F_a (N) is found as follows:

$$F_a = F_{a1} + F_{a2} \quad (2.4)$$

The torques M_v and M_r (Nmm) due to cutting and radial force respectively are as follows:

$$M_v = F_{v1} \frac{D}{2} = F_{v2} \frac{D}{2} \quad (2.5)$$

$$M_r = F_{r1} 2w = F_{r2} 2w \quad (2.6)$$

Thus, the resultant torque M (Nmm) is calculated as:

$$M = M_v - M_r \quad (2.7)$$

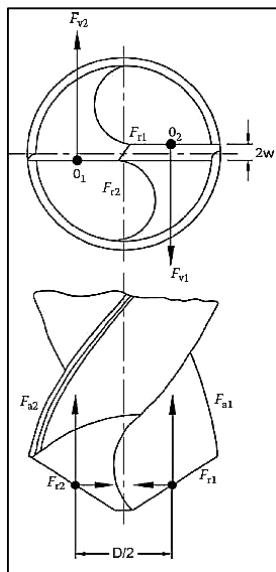


Figure 2.4. Components of the drilling forces in drilling process [33].

For a properly sharpened cutting edges of a drill bit, it can be supposed that;

$$F_{v1} = F_{v2} = F_v \quad (2.8)$$

and

$$F_{a1} = F_{a2} = F_a \quad (2.9)$$

In case the drill is not sharpened properly, it may result in nonlinear holes due to the effect of the lateral forces which leads to lateral drift of the drill.

The main cutting force F_v acting on each cutting lip of the drill can be calculated as follows:

$$F_v = k_s A_c \quad (2.10)$$

where, k_s (N/mm²) is the specific cutting energy and A_c (mm²) is the chip cross-sectional area, which is shown as follows,

$$A_c = \frac{f}{2} \times \frac{d}{2} = \frac{fd}{4} \text{ (mm}^2\text{)} \quad (2.11)$$

$$A_c = bh \quad A_c = \frac{bf}{2} \sin x \quad (2.12)$$

This formula can be also determined as follows:

$$F_v = k_s \frac{fD}{4} = k_s bh \quad (2.13)$$

$$b = \frac{D}{2\sin(x)} \quad (2.14)$$

Where f (mm/rev) is feed, D (mm) is the drill diameter, b (mm) is the undeformed chip length h (mm) is the chip thickness to be removed by each drill lip and $X(^{\circ})$ is the drill lip angle, Figure 2.5.

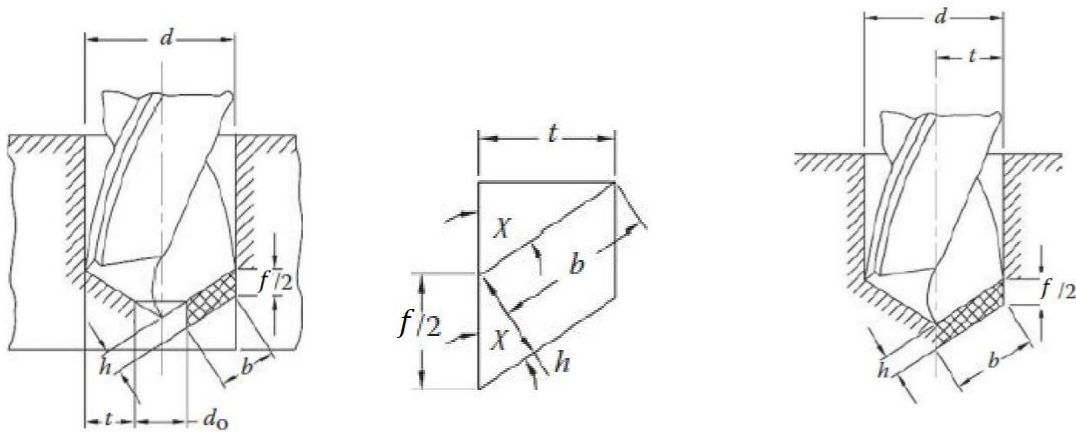


Figure 2.5. Elements of undeformed chip in drilling [33]

In most of the cases, radial force components F_{r1} and F_{r2} are assumed to counterbalance each other. Thus, M_r is equal to zero, and

$$M = M_v = F_v \frac{D}{2} \quad (2.15)$$

$$M = k_s \left(\frac{fD}{4} \right) \left(\frac{D}{2} \right) = k_s \frac{fD^2}{8} \quad (2.16)$$

The total drilling power, N_t (kW) can be calculated as follows:

$$N_t = N_c + N_{fd} \quad (2.17)$$

Where, N_c (kW) is the main drilling (cutting) power and N_{fd} (kW) is the feed power. If the N_{fd} is assumed to be equal to zero, N_t is equal to N_c . N_t (kW) can be also expressed as [33]:

$$N_t = N_c = \frac{F_v V}{60 \times 10^3} = \frac{k_s f D V}{4 \times 60 \times 10^3} \text{ (kW)} \quad (2.18)$$

Many process parameters affect the drilling torque M and the thrust force F_a . They are related with workpiece material, drill geometry and drilling conditions as listed in Figure 2.6.

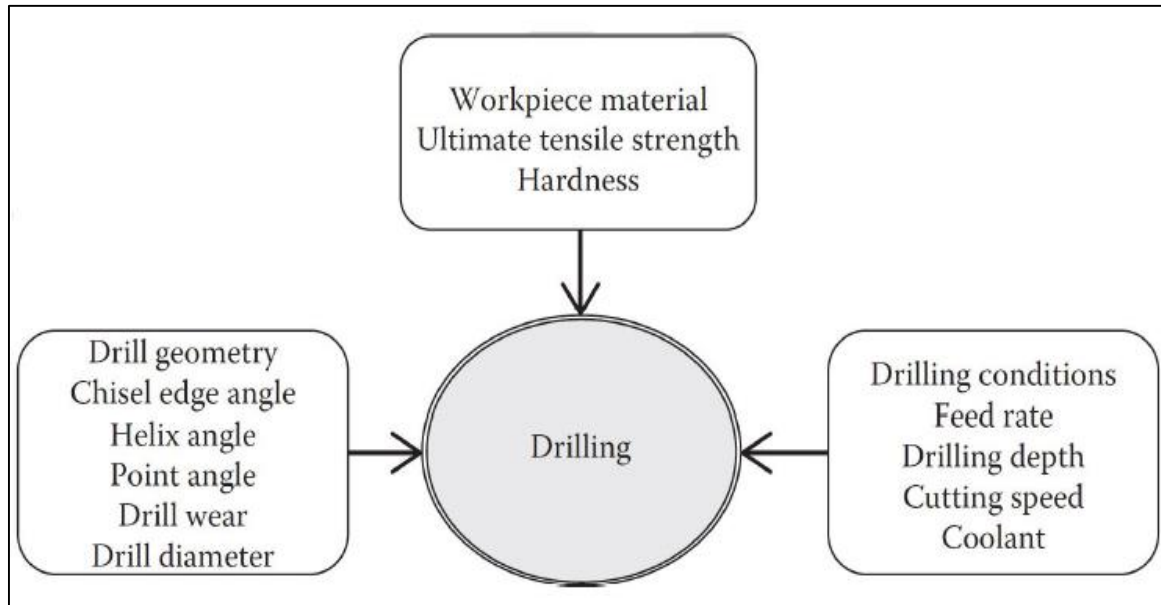


Figure 2.6. Factors affecting the drilling forces [33].

2.5. Tool Wear

Using optimal cutting conditions and selection of cutting tool materials are very important, because very hard cutting conditions oppose the twist drill due to great heat generation and cutting forces.

Thermal failure may happen in case of too high cutting temperatures, due to softening of the tool point and changing the geometry of the cutting edges. In case of too high thrust force and torque, fracture failure happens. Besides, gradual tool wear and the desired wear mode, can provide tool life as long as possible [1].

Chisel edge wear occurs at the tip of the drill bit and originates from chisel edge abrasion or plastic deformation. This type of wear leads to increase the thrust forces two or three times and centering errors.

Flank wear occurs through the flank face of the drill bit and originates mainly from abrasion.

Flank wear increase causes the increase in the thrust force, the power consumption and the cutting temperature. Elevated temperature accelerates the flank wear because of the thermal softening effect. In addition, flank wear leads to the increases in the burr heights at the hole exit when drilling through holes.

Margin wear occurs at the outer corner of the drill which is in contact with machined surface, and originates from abrasion, thermal softening, or diffusion. Increased margin wear causes hole diameter errors and undesirable surface roughness of the holes.

Crater wear occurs at the flute surface of the drill bit and originates from thermal softening or diffusion. Excessive crater wear may lead to deformation of the cutting edge, chipping or drill failure.

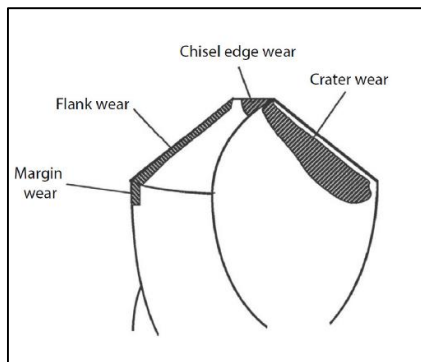


Figure 2.7. Characteristic wear types and wear regions of a twist drill [34].

Cutting speed directly affect the tool life. Abrasive wears mostly take place on outer corners of a twist drill at low and moderate cutting speeds. While at higher speeds abrasive and adhesive wears are observed.

Generally higher cutting speeds affect negatively on tool life. But instead of changing the cutting parameters (cutting speed and feed rate), changing the tool material to one having higher hot hardness, can improve the cutting tool performance. Also, a good increase in tool life can be provided using coated drills.

Several reasons can cause the failure of the drill and chipping such as overloading, vibrations, chip packing, misalignment and tool defects, hard points in workpiece material, etc. [34].

The wear types occurred on solid carbide drills in drilling operation are illustrated in Figure 2.8. with causes and solution suggestions to reduce the related tool wear.

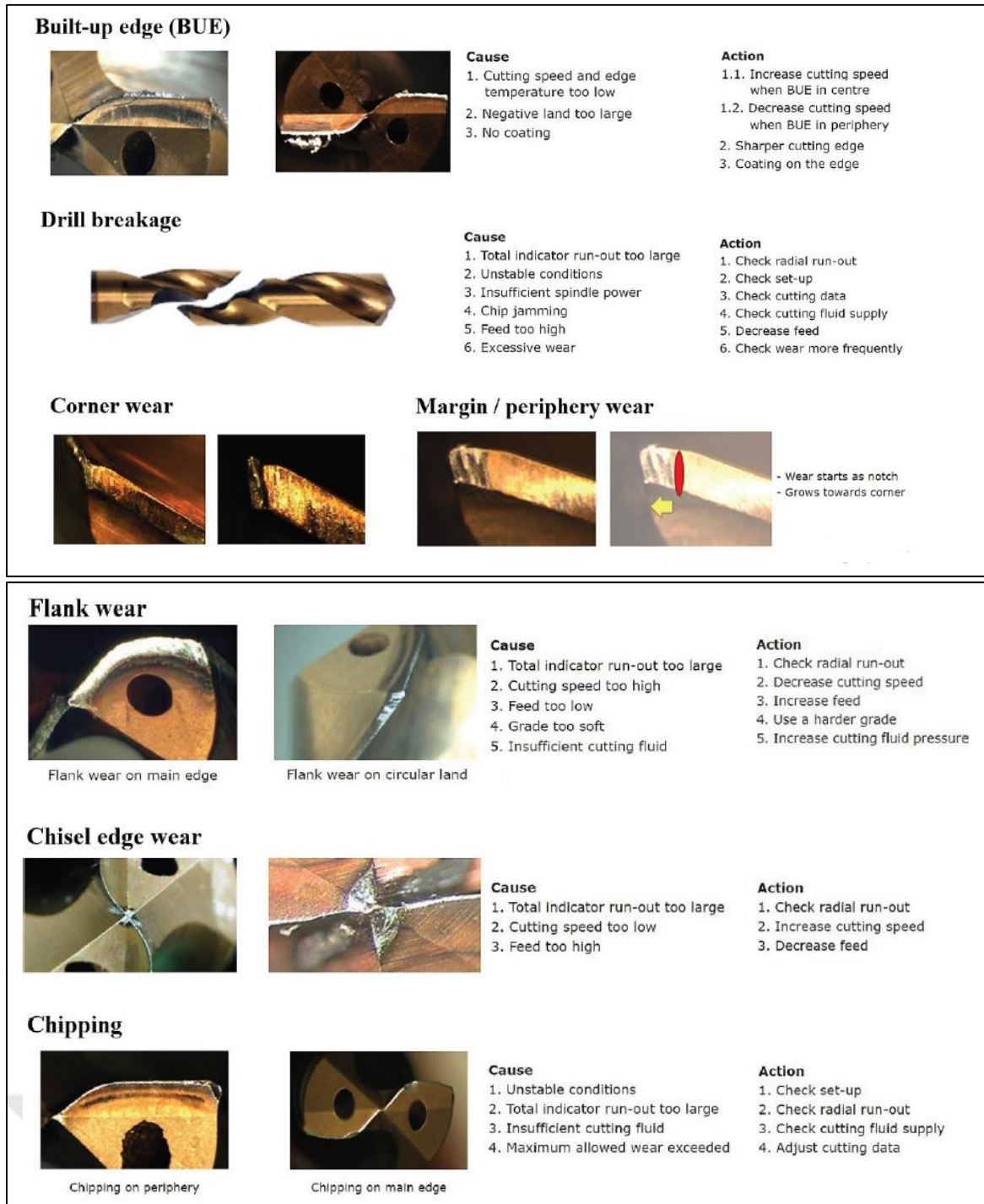


Figure 2.8. The different wear types on the carbide drills [25].

2.6. Cutting Temperature

A great amount of energy is spent in machining operations for material removal. Nearly all of this energy is converted into heat and this causes high temperatures in the cutting zone. The machining performance is directly affected by these high temperatures. Generally the

cutting tool and workpiece material properties, tool life, cutting forces, machined surface quality and cutting forces are affected by cutting temperatures.

In drilling, thermal conditions differ from the other machining operations such as turning, boring, etc. because chip formation occurs inside the hole and the chip keeps being in contact with the drill for a long time, which results in an increase in tool temperatures. Because of that, the cutting temperatures are further increased with the motion of the cutting tool. In general, cutting temperatures do not become a steady state in drilling, and increase with increasing hole depth. This situation limits the maximum hole depth for particularly difficult-to-cut materials such as Inconel 718.

Lastly, the temperatures vary along cutting edges of the drill, because the cutting speed is lower at the cutting edges close to center of the drill. Therefore, outer corners or margin of the drill has higher rotational speed and cutting temperatures during a drilling operation [34].

3. MATERIAL AND METHOD

3.1. Material

3.1.1. Workpiece material and model

For Inconel 718 superalloy, the material limiting chemical composition is given in Chapter 1.

For Incoloy A286 superalloy, the chemical composition of the material which is taken from the certificate of the material (see Attachment 1), is given in Table 3.1

Table 3.1. Chemical composition of Incoloy A-286 Superalloy.

Elements	Ni	Cr	Mo	B	P	Al	Ti	C	Mn	Si	V	S	Fe
Percentage %	25.2	14.79	1.28	0.003	0.014	0.18	2.28	0.05	1.11	0.02	0.19	0.02	Balanced

According to the certificate, the workpiece material has been solution treated by holding for one hour at 980 °C, then cooled and age hardened by holding for 16 hours at 720 °C then cooled in air.

The data recorded in the certificate also shows that, the tensile strength of the material is 925 MPa, yield strength is 580 MPa and it has an elongation of 15 percent.

The workpiece for Inconel 718 was modeled as a disc with a diameter of 7 mm and a thickness of 2,5 mm. And the workpiece for Incoloy A286 was modeled as a disc that has a diameter of 10 mm and a thickness of 3 mm.

Pre-machined blind cone shaped hole having same dimensions with the conical end of related drill bit was also generated on both materials's workpiece models. Thus, full cutting process starts with full hole diameter size at the beginning, without waiting drilling of conical part. As a result, computation time decreases considerably. As a facility of the Deform 3D, the conical hole can be prepared exactly from the imprint of drill bit as shown in Figure 3.1.

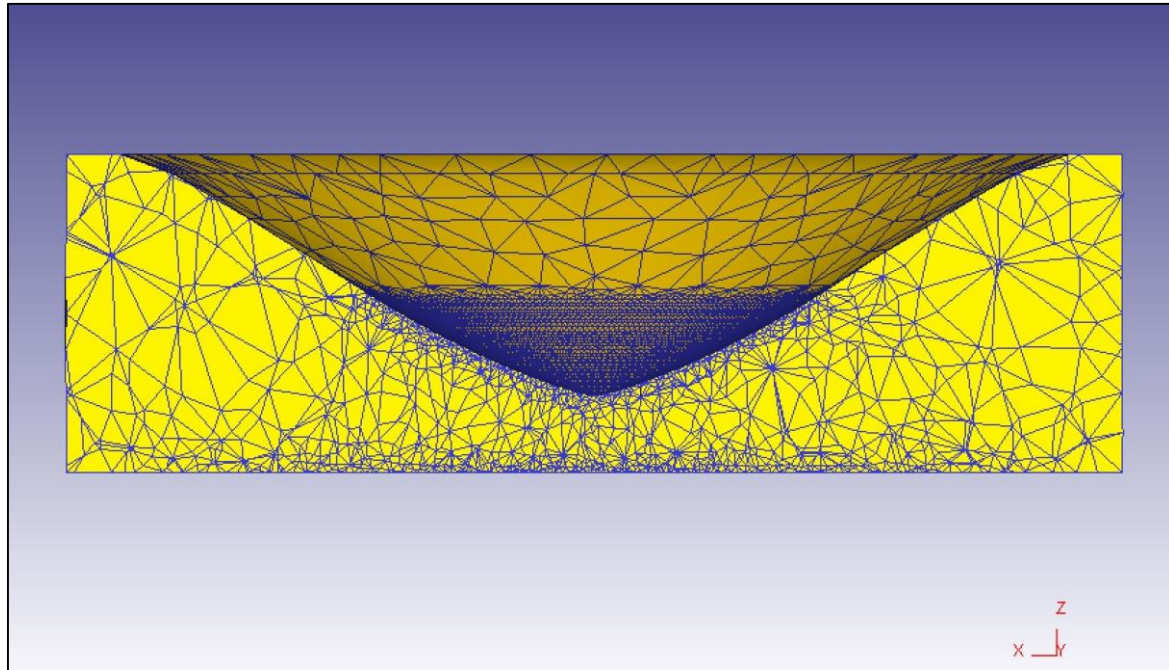


Figure 3.1. Workpiece model cross-section

This way, the FEM simulation time is further reduced, because the space between the cutting edges of the twist drill and the workpiece is minimized so that the machining process starts immediately at full load [35]. For achieving accepted results of thrust force and torque, the conical part of the twist drill must be completely engaged with the workpiece. So that preparing a pre-machined hole decreased the run time dramatically to reach this point. In each case the depth of the pre-machined conical hole measured on the drill axis, is adjusted to be a bit smaller than the height of the conical end of the drill bit, so that after a specific number of rotation which is related to the feed rate, drill's conical end completely entered the workpiece.

3.1.2. Drill geometry, material and model

For drilling operation simulations of Inconel 718 superalloy, a 5 mm diameter twist drill with a point angle of 140 degrees, helix angle of 30 degrees was modeled in the Deform 3D software. 15% Cobalt uncoated carbide was selected as tool material (see Figure 3.2).

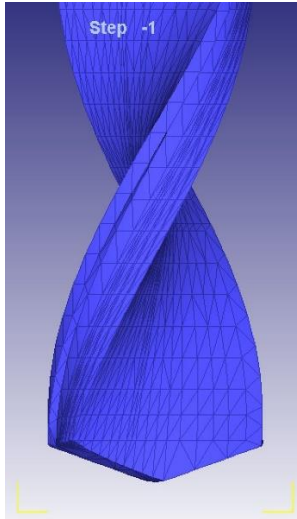


Figure 3.2. 5 mm diameter drill model

Twist drill mesh properties and other related assumptions made in the FEM analysis of Inconel 718 are given in Table 3.2.

Table 3.2. Twist drill mesh properties for Inconel 718

Assumptions	Values
Tool Material	Carbide %15 Cobalt
Mesh Size Ratio	4
Element Type	Tetrahedral
Mesh Type	Fine Mesh
Surface Polygons	4,296
Nodes	2,150 nodes
Relative Mesh Type	32,000

For drilling simulations of Incoloy A286, two different genuine carbide twist drill bits purchased from the market were modelled as described in the following. These drill bits are identical with those used in an experimental study [30] present in the literature. The drill bit dimensions and coating materials are given in Table 3.3. Their technical drawing is also presented in Attachment 3.

Table 3.3. Twist drill geometries and coating materials for Incoloy A286

Point Angle	Helix Angle	Diameter	Coating
120°	28°	8.38 mm	TiN
140°	28°	8.38 mm	TiN

Since the CAD model of the twist drills could not be obtained, it was decided to scan drill bits with 3D scanning camera systems and design the drills using reverse engineering. Then

twist drill models were designed in SOLIDWORKS (Figure 3.3.) and compared to the 3D scanned models in Geomagic Design X program, until we obtained the models as close to the real drills as possible.

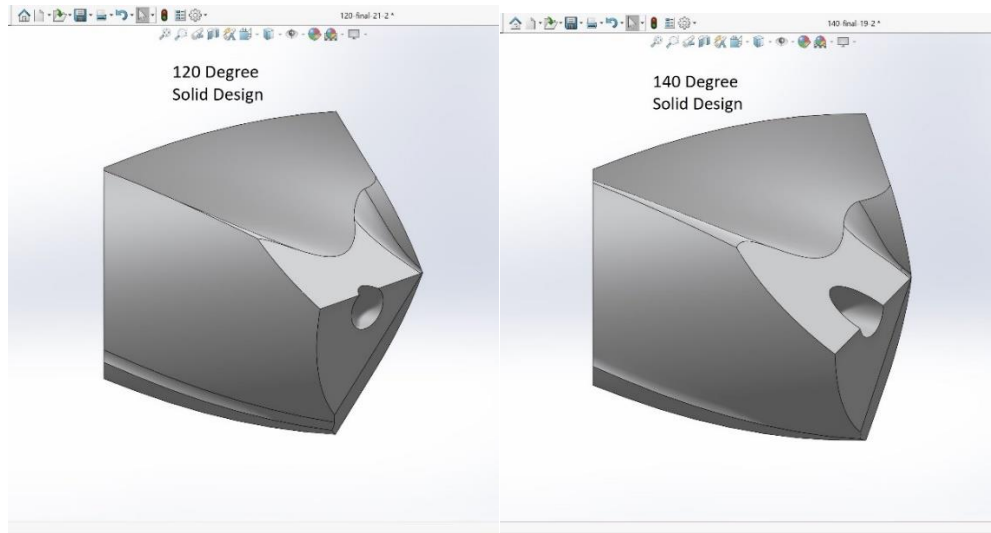


Figure 3.3. Twist drills designed in SolidWorks

The drills were scanned in the laboratories of Gazi University using AICON Smart Scan 3D system, Figure 3.4. The metallic surface of the drills were painted using special powder spray for 3D cameras for good light reflection, Figure 3.4. The solid models designed in SolidWorks, were compared to the scanned models and the difference between them was minimized, Figure 3.5 and Figure 3.6.



Figure 3.4. AICON Smart Scan 3D system during scanning process

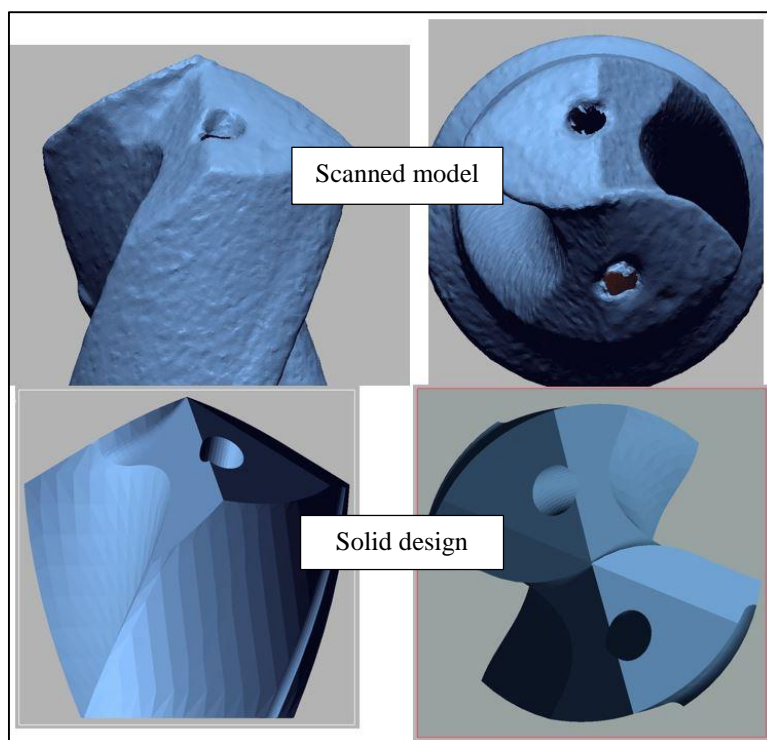


Figure 3.5. Twist drill with 120 degree point angle compared to scanned model

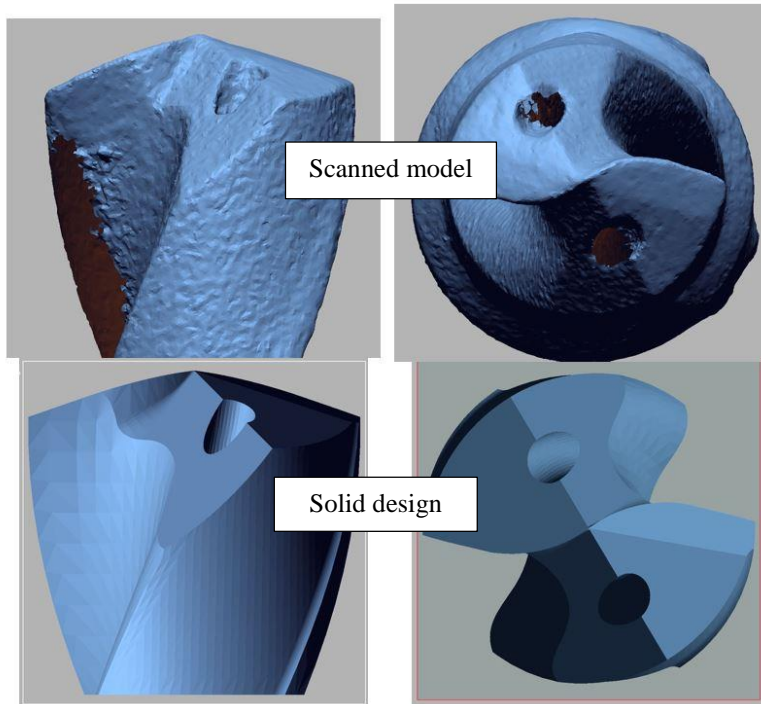


Figure 3.6. Twist drill with 140 degree point angle compared to scanned model

3.1.3. Cutting conditions in the simulations

For modeling drilling operations of Inconel 718 superalloy, an uncoated twist drill with a point angle 140 degrees was used. The Table 3.4, illustrates the operation plan for the numerical work when using two different cutting speeds and two different feed rates for drilling both aged and annealed Inconel 718.

Table 3.4. Simulation plan for drilling of aged and annealed Inconel 718

No. of Operations	Cutting Speed (m/min)	Feed Rate (mm/rev)
1	10	0.05
2	10	0.1
3	20	0.05
4	20	0.1

For modeling drilling operations of Incoloy A286 superalloy, two different twist drills with point angles 120 and 140 degrees with coating material (TiN) were used. The Table 3.5, illustrates the operation plan for the numerical work when using two different cutting speeds with two different feed rates.

Table 3.5. Simulation plan for drilling of Incoloy A286

Operation No	1	2	3	4	5	6	7	8
Drill Point Angle	120	120	120	120	140	140	140	140
Coating Material	TiN	TiN	TiN	TiN	TiN	TiN	TiN	TiN
Feed mm/rev	0.05	0.05	0.1	0.1	0.05	0.05	0.1	0.1
Cutting Speed m/min	25	50	25	50	25	50	25	50

3.1.4. The Software program used for the numerical simulations

FEM based program DEFORM 3D has been used for the numerical simulations of drilling Incoloy A286 superalloy. DEFORM is one of the most known software programs used for forming and machining simulations.

In this study, Version 11 of the software program was used which is the latest version available until the time of preparing this thesis.

3.2. Method

Finite element models used for simulation of metal cutting operations, include the constitutive model parameters which represents the dynamic behavior, mechanical, physical and thermal properties of the workpiece material and the cutting tool material. The parameters entered also represent the contact conditions like friction and heat transfer coefficients. However, representing work material behavior under high strain, strain rate, and temperatures, is the most important of these constitutive material model parameters, [28]. And it is applicable to high rate deformation of many materials including Inconel 718 and Incoloy A286 superalloys.

In the numerical simulations of drilling operation, Johnson-Cook constitutive material model, Eqn. (3.1) was applied. [36]

$$\bar{\sigma} = [A + B\bar{\epsilon}^n] \left[1 + C \ln \left(\frac{\dot{\bar{\epsilon}}}{\dot{\bar{\epsilon}}_0} \right) \right] \left[1 - \left(\frac{T - T_{room}}{T_m - T_{room}} \right)^m \right] \quad (3.1)$$

where; $\bar{\sigma}$ is the equivalent stress (MPa), $\bar{\epsilon}$ is the equivalent plastic strain, $\dot{\bar{\epsilon}}$ is the equivalent plastic strain rate (s⁻¹), $\dot{\bar{\epsilon}}_0$ is the reference equivalent plastic strain, T is the temperature (°C), T_m is the workpiece material melting temperature, T_{room} is the room temperature (for Incoloy A286, 30°C based on the environment temperature when the tests performed), **A** (yield strength), **B** (strain hardening coefficient), **C** (strain rate hardening coefficient), **n**

(*strain rate hardening exponent*) and m (*thermal softening exponent*) are the J-C model constants.

Many researchers have determined J-C parameters for Inconel 718. It is clearly observed that the J-C parameters depend on the material type, i.e. type of heat treatment applied. In this study, aged and annealed types of Inconel 718 were selected to use in the drilling operation simulations.

The J-C model parameters used in this study for both aged and annealed Inconel 718 were taken from the study of T. Ozel et al [28], and are shown in Table 3.6. They have referred the J-C parameters for aged Inconel 718 to Lorentzon et al. (2009) [47], and referred the J-C parameters for annealed Inconel 718 to Uhlmann et al. (2007) [48]. The yield strength values of aged and annealed Inconel 718 are 1241 MPa and 450 MPa respectively.

Table 3.6. Johnson-Cook model parameters for Inconel 718 [28]

Heat Treatment	A (MPa)	B (MPa)	C (-)	N (-)	M (-)	$\dot{\epsilon}_0$ (s ⁻¹)
Aged	1241	622	0.0134	0.6522	1.3	1
Annealed	450	1700	0.017	0.65	1.3	0.001

But for Incoloy A286 superalloy, the J-C parameters were not available in the literature, therefore as one of the main goals of this study, the parameters were determined in the scope of this study through Split Hopkins and tensile tests.

3.3. Experimental Tests And Johnson-Cook Parameters Determination For Incoloy A286

3.3.1. Quasi-static tension tests

To obtain the parameters of the first term of the Johnson-Cook material model which may be obtained from quasi-static tests, quasi-static tests were performed in the scope of this thesis. As it is known, tension tests are the most widely used techniques for testing materials at quasi-static strain rates. Although it is a very basic test, it provides important knowledge about selecting materials for engineering applications, [39].

Tensile test specimen shape shown in Figure 3.7, are specified by ISO (International Organization for Standardization) standards. The dogbone specimen prepared for a tension test, is mounted on the grips of the tensile test machine and elongated at a constant crosshead

speed. During this process, applied load and elongation of the test specimen are recorded using mechanical extensometers or cameras. Then to construct the stress-strain behavior of the material, the recorded force and displacement data are used.

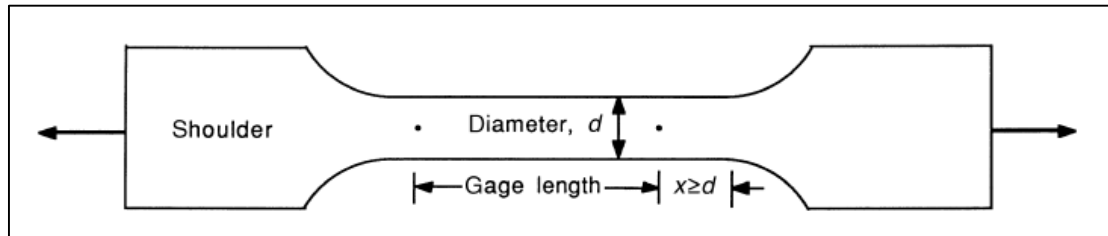


Figure 3.7. Typical dogbone specimen [39].

3.3.2. Dynamic tests

Split Hopkinson pressure bars are the most reliable and used devices for material characterization at higher strain rates. Dynamic tests performed by these devices are classified as compression, tension and torsion according to the loading conditions. Split Hopkinson Pressure Bars (SHPB) also known as Kolsky Bars [40].

3.4. Background on Split Hopkinson Pressure Bar

3.4.1. A brief history about Split Hopkinson pressure bar

In 1914 Bertram Hopkinson invented a pressure bar to measure the pressure produced by high explosives and or high speed impact of bullets [40]. To record the movements of cylinders, Hopkinson used pendulums with a pencil and paper in order to obtain a pressure – time curve produced by detonation of the gun cotton as shown in Figure 3.8.

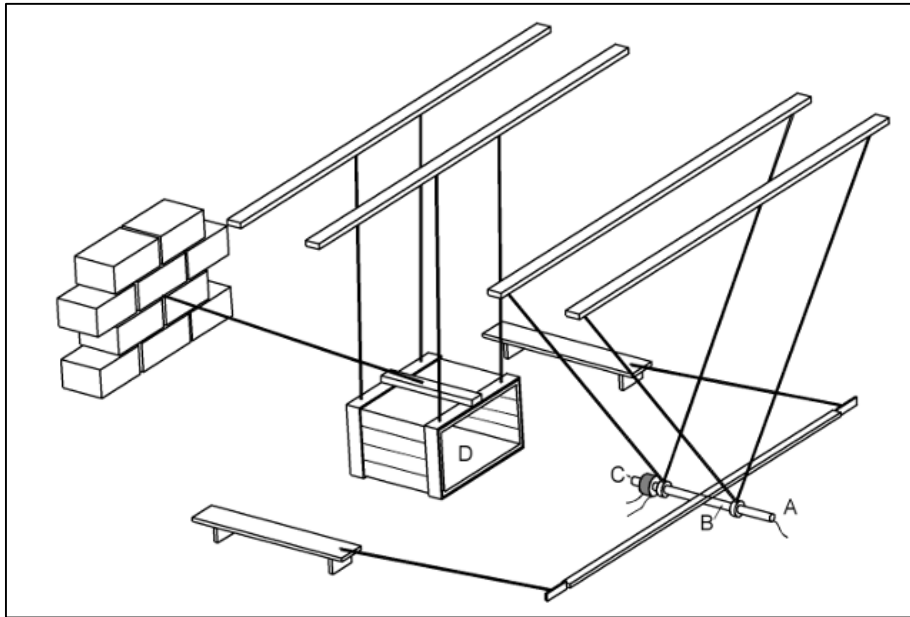


Figure 3.8. The Hopkinson experiment [40].

In 1948, Davis used parallel plate and cylindrical condenser microphones to electrically measure the axial and radial movements of the bar loaded by the detonation as shown in Figure 3.9. Assuming the pressures in the bars to be under the elastic limit of the material, the output from the condenser is proportional to the displacement - time relations [41]. These electrical measurements are more accurate than Hopkinson's method. Davis also studied the dispersion of the stress waves' propagating in a long rod.

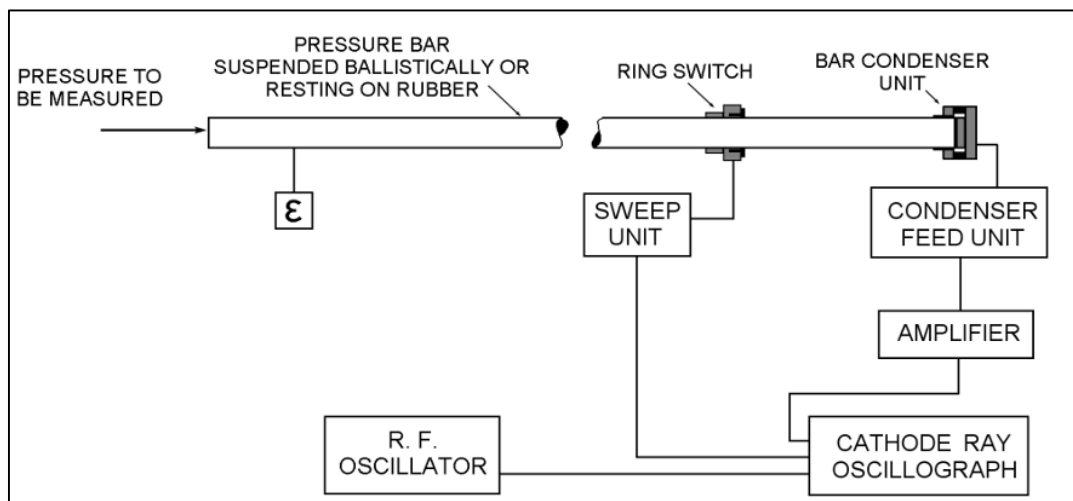


Figure 3.9. Davis experiment [40].

In 1949, Kolsky extended the technique to measure stress – strain response of materials under impact loading conditions, by adding a second pressure bar to Hopkinson's device.

This was the main difference between Kolsky bar and Davis bar, in which Kolsky used two bars where a specimen was sandwiched in between as illustrated in Figure 3.10.

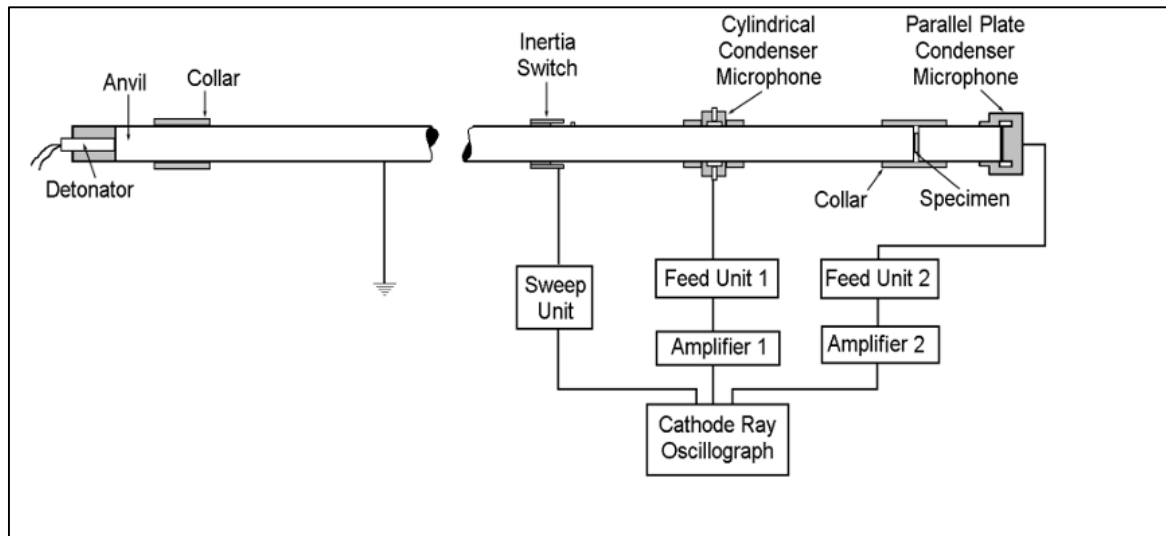


Figure 3.10. The Kolsky bar [40].

To calculate material properties based on strain rate in the bars, Kolsky presented some expressions. Kolsky's technique also is called Split Hopkinson Bar in the memory of Bertram Hopkinson.

To measure the strains in the two bars of SHPB, in 1954 Krafft firstly mounted strain gauges instead of condenser microphones [41]. He also used a gun to launch a projectile, a striker bar, to impact on the incident bar. Obtaining trapezoidal shaped pulse which have been recognized ideal for Kolsky bar experiments, is from the advantages of using a striker.

In 1964, Lindholm introduced an updated version of the SHPB and presented as a valid dynamic characterization tool. This apparatus became popular in laboratories around the world. Nowadays, there are still new improvements with recent technological devices in SHPB [46].

3.4.2. Split Hopkinson pressure bar apparatus

A general Split Hopkinson Pressure (Kolsky) Bar consists of three major components which are, a loading device, incident and transmitted bars and data acquisition system as illustrated in Figure 3.11.

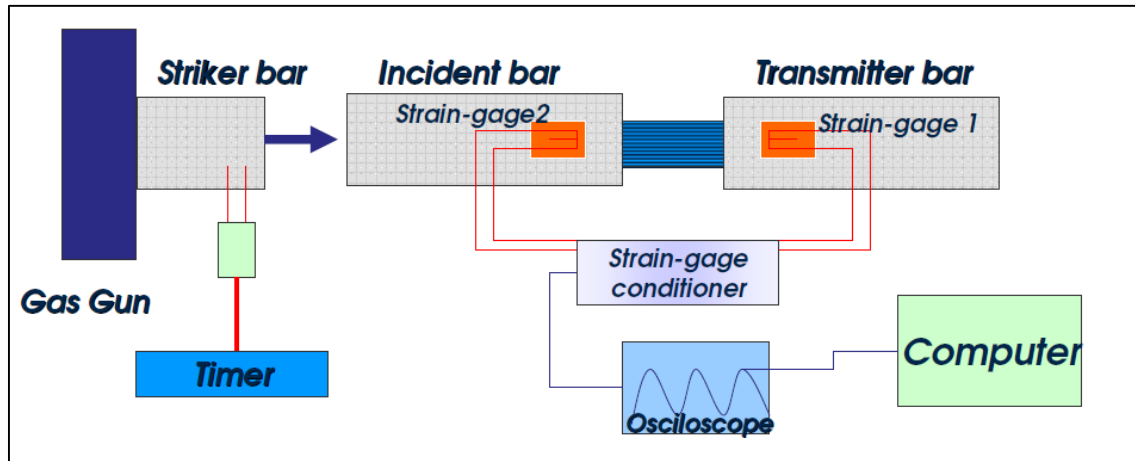


Figure 3.11. The schematic view of SHPB [42].

The loading should be controllable in SHPB experiments. Launching a striker to impact the incident bar, is the most common method for dynamic loading. A gas gun and pressure vessels are generally used for this purpose. A sudden release of the compressed air in a pressure vessel launches the striker and then accelerates along the gun tube to impact the end of the incident bar. When the striker impacts the incident bar with an initial impact velocity, a compressive wave is formed in the incident bar. The amplitude of this compressive wave is directly proportional with the impact velocity. When the compressive wave propagates through the incident bar, it comes to the interface between incident bar and sandwiched specimen. At this location, a part of compressive wave is reflected back through the incident bar while the rest of the wave is transmitted into the specimen. Strain gauges in a data acquisition system are used to measure the incident and transmitted strains on the pressure bars [43].

3.5. Quasi-Static Tensile Test Procedure

Tensile test specimens were prepared from the workpiece materials of Incoloy A286 superalloy provided, and quasi-static tensile tests were carried out to determine the relevant J-C parameters for the material. Figure 3.12 shows shape and dimensions of the tensile test specimens.

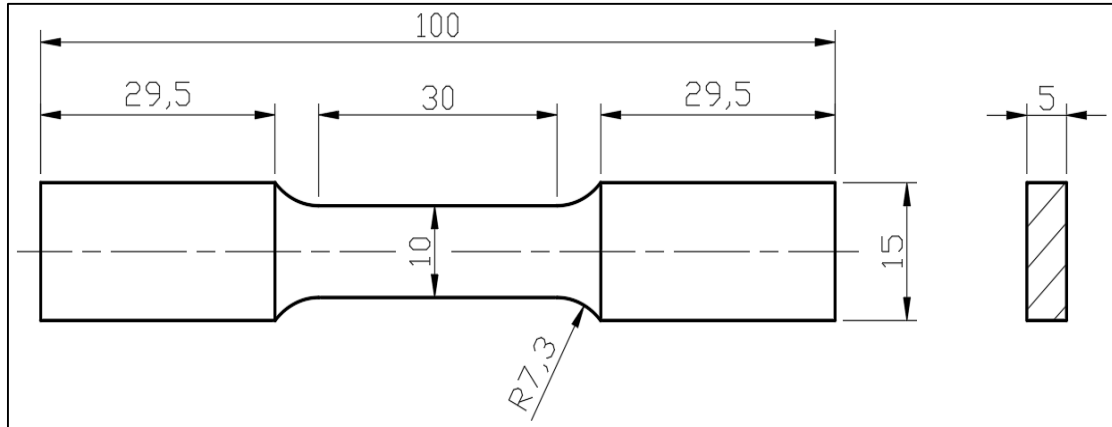


Figure 3.12. Tensile test specimen, dimensions in (mm)

The quasi-static tension tests were performed in the laboratories of *Ion Metal Materials Testing Laboratory* located in METU Campus/Ankara. Tensile tests were performed with a strain rate of 0.000083 s^{-1} at a room temperature of $30 \text{ }^{\circ}\text{C}$. The pictures of tensile test specimen mounted on the grips of the tensile test machine before and after testing are shown in Figure 3.13. Tested (fractured) test specimens pictures are also shown in Figure 3.14

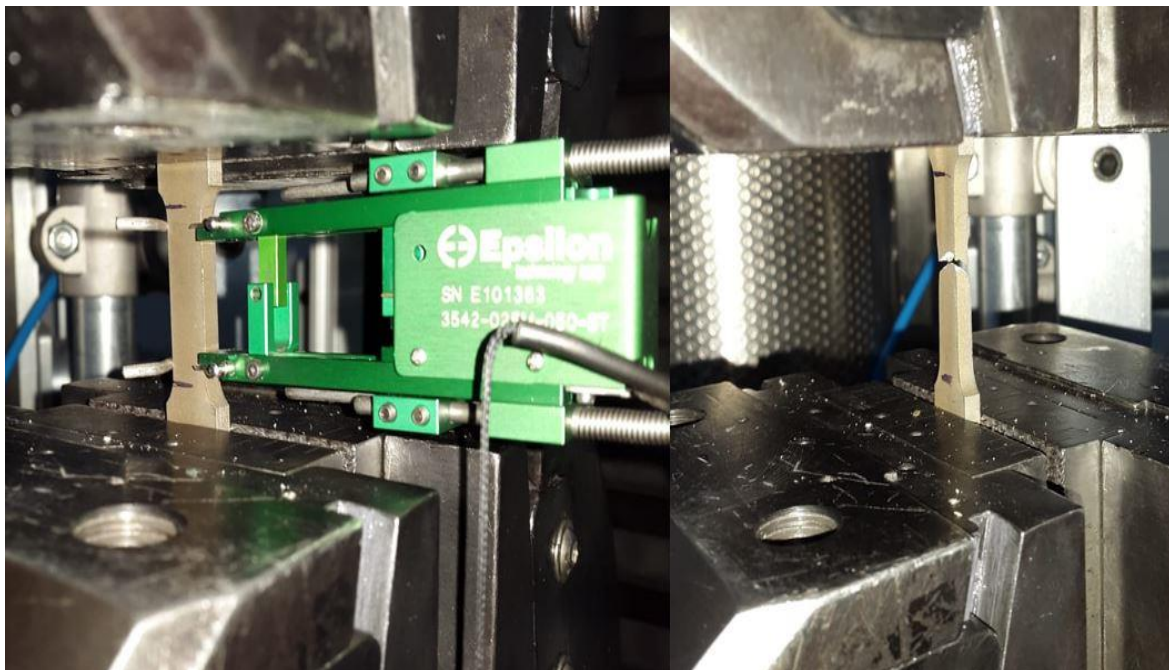


Figure 3.13. The pictures of tensile test specimen mounted on tensile test machine before (at left) and after (at right) testing



Figure 3.14. Pictures of tested tensile test specimens

The expression in the first set of brackets of J-C constitutive material model given in Eqn. (3.1) characterize the strain hardening effect and given once again as follows.

$$\bar{\sigma} = [A + B\bar{\epsilon}^n][\dots \dots \dots][\dots \dots \dots] \quad (3.2)$$

where **A** is the yield strength, and determined from quasi-static tensile test. **B** (strain hardening coefficient) and **n** (strain rate hardening exponent) were calculated by using Microsoft Excel Solver, from the true stress-true strain curve (Figure 3.15) obtained from the quasi-static tensile test data.

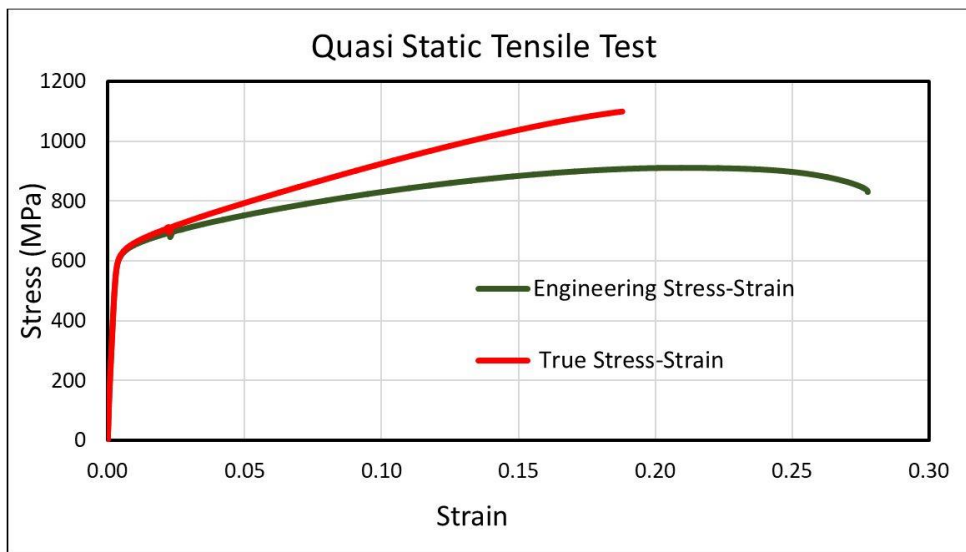


Figure 3.15. Engineering and true stress-strain curves for quasi-static tensile test

3.6. Dynamic Compression Test Procedure

Dynamic compression test specimens were prepared from the workpiece materials of Incoloy A286 superalloy provided, and dynamic compression tests were carried out to determine the relevant J-C parameters for the material. Dynamic compression test specimens were prepared as $\text{Ø}6 \text{ mm} \times 6 \text{ mm}$ compact cylinders using wire erosion machine, Figure 3.16.

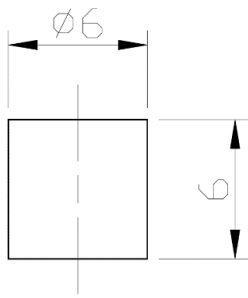


Figure 3.16. Cylindrical dynamic compression test specimen, dimensions in (mm)

Dynamic compression tests were performed in the laboratories of Tübitak SAGE (Defense Industries Research and Development Institute) using Split Hopkinson pressure bar machine, see Figure 3.17. A snapshot from the high temperature dynamic compression test is shown in Figure 3.18. The heating of the the specimen sandwiched between the incident and transmitter bars can be observed from the picture. The temperature of the specimen is measured with a portable thermocouple thermometer.



Figure 3.17. Split Hopkinson pressure bar machine

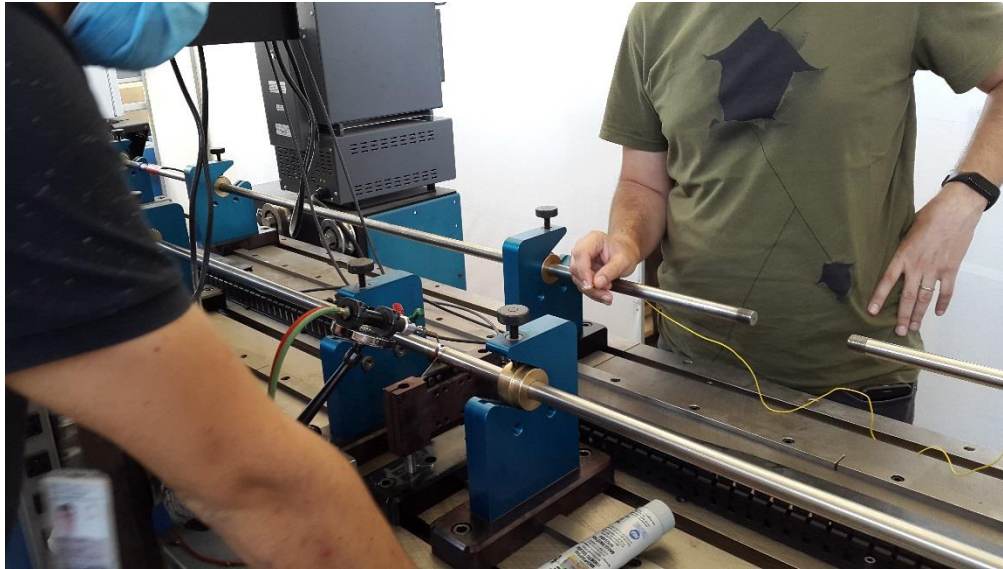


Figure 3.18. Performing the high temperature dynamic compression test in Split Hopkinson pressure bar machine

The dynamic compression tests performed at room temperature (30 °C) and at high temperature (270 °C) are listed in Table 3.7. As can be seen from Table 3.7, three tests were performed for each strain rate using the Split Hopkinson pressure bar test machine. It should be noted here that the failed tests were repeated and at least three successful tests were performed for each strain rate value.

Figure 3.19 shows the pictures of tested cylindrical specimens in high strain rate dynamic compression tests. As a result of dynamic compression tests, as expected, the lengths of specimens decrease, while the diameters increase.

Table 3.7. Room temperature (30 °C) and high temperature (270 °C) dynamic compression tests

Test No.	Temperature (°C)	Strain Rate (s ⁻¹)
1,2,3	30	80
4,5,6	30	615
7,8,9	30	1180
10,11,12	30	1530
15,16,17	270	625
Specimen Dimensions: Ø6 mm X 6 mm cylindrical		



Figure 3.19. Pictures of tested cylindrical specimens in dynamic compression tests

The expression in the second set of brackets of J-C constitutive material model given in Eqn. (3.1) characterize the strain rate hardening effect and given once again as follows.

$$\bar{\sigma} = [\dots \dots \dots] \left[1 + C \ln \left(\frac{\dot{\epsilon}}{\dot{\epsilon}_0} \right) \right] [\dots \dots \dots] \quad (3.3)$$

Strain rate hardening coefficient C , in this expression, was calculated by using Microsoft Excel Solver, from the true stress-true strain curves (Figure 3.20) obtained from the room temperature dynamic compression tests data.

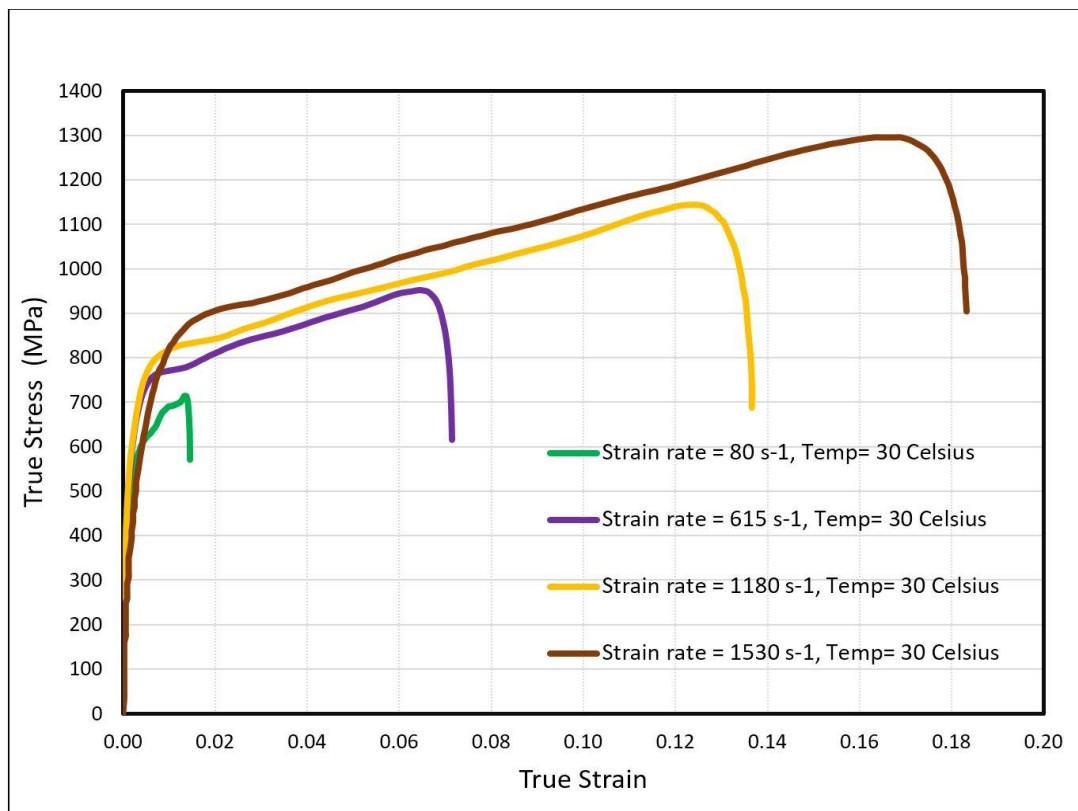


Figure 3.20. High strain rate dynamic compression tests at room temperature

The expression in the third set of brackets of J-C constitutive material model given in Eqn. (3.1) characterize the thermal softening effect and given once again as follows.

$$\bar{\sigma} = [\dots \dots \dots][\dots \dots \dots] \left[1 - \left(\frac{T - T_{room}}{T_m - T_{room}} \right)^m \right] \tag{3.4}$$

Thermal softening exponent **m**, in this expression, was calculated by using Microsoft Excel Solver, from the true stress-true strain curves (Figure 3.21) obtained from the high temperature dynamic compression tests data.

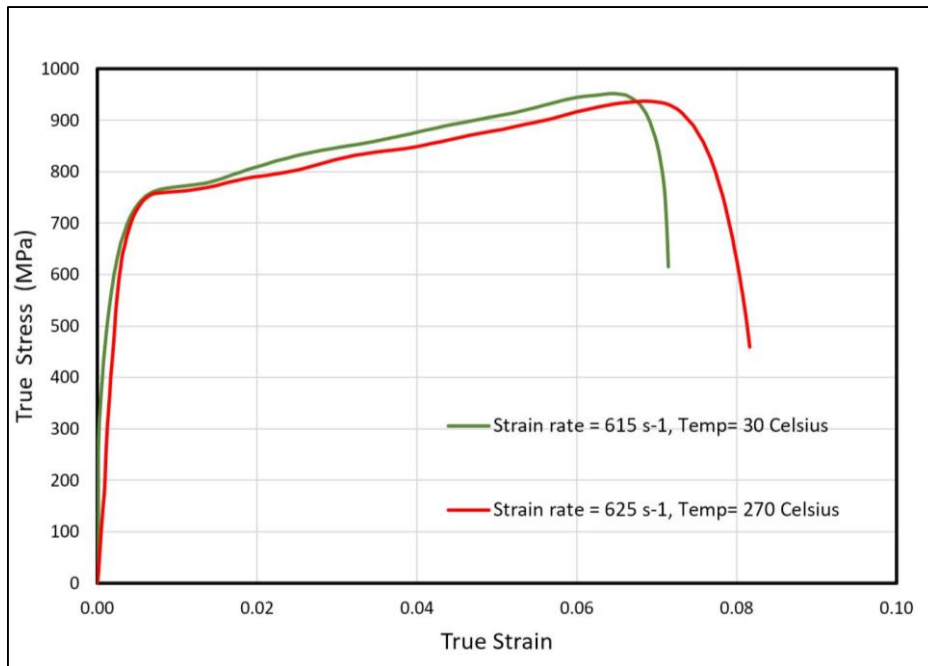


Figure 3.21. High strain rate dynamic compression tests at room (30 °C) and high (270 °C) temperature

All of the Johnson-Cook constitutive material model parameters determined from the experimental data, as described above, for Incoloy A286 are given in Table 3.8.

Table 3.8. The J-C parameters determined for Incoloy A286

J-C Parameters	A (Mpa)	B (Mpa)	C	n	m
Values	621	1712	0.014117	0.729933	1.37

In order to show to what extent the J-C model curves, obtained with the determined parameters, fit the experimental data, two examples are given: First, J-C model curve and experimental curve are shown together in Figure 3.22 for room temperature (30 °C) dynamic compression test at strain rate of 1530 s-1. Second, J-C model curve and experimental curve

are shown together in Figure 3.23 for high temperature (270 °C) dynamic compression test at strain rate of 625 s⁻¹. As can be seen from both figures, JC model curves fit the experimental results fairly well.

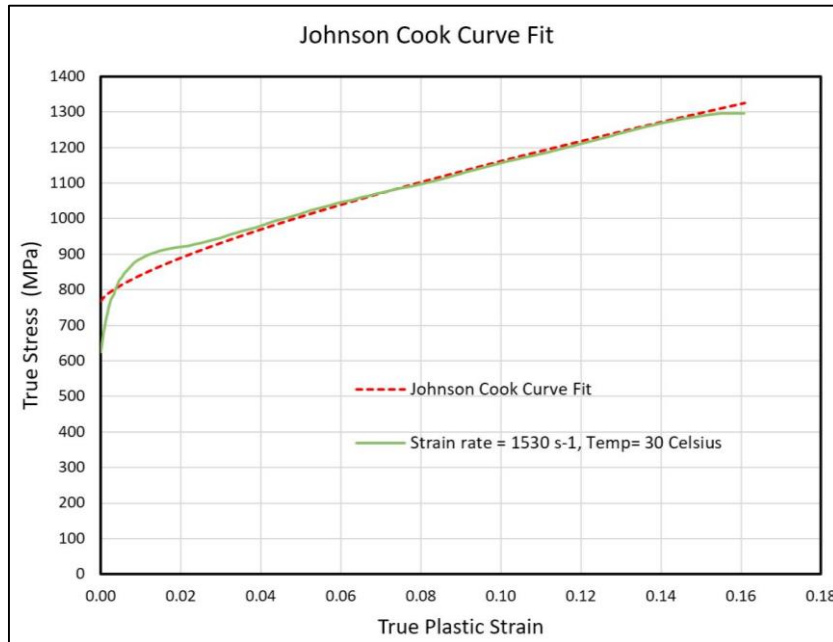


Figure 3.22. J-C curve fit for dynamic compression test at room temperature

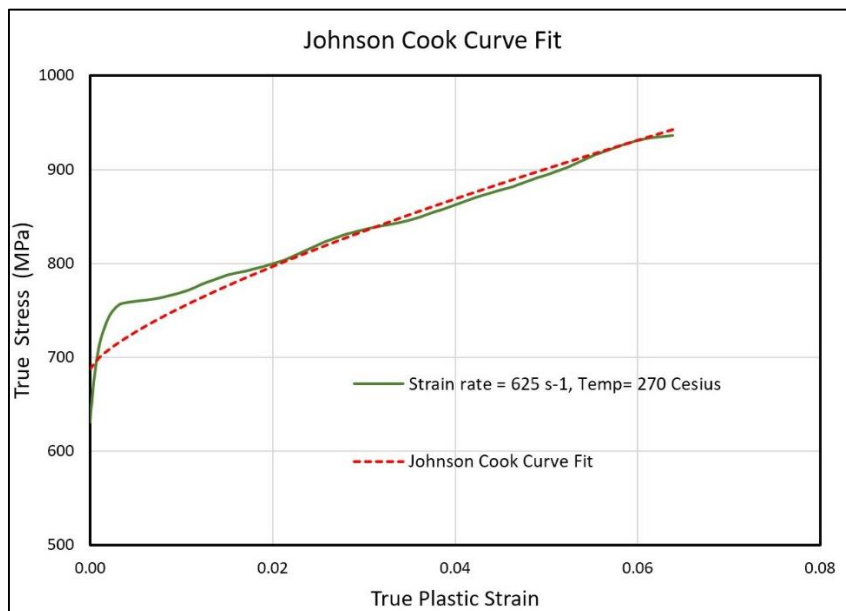


Figure 3.23. J-C curve fit for dynamic compression test at high temperature

3.7. Numerical Simulations

The J-C model curves for aged and annealed Inconel 718 and for Incoloy A286 were fitted using their J-C parameters, given in Table 3.6 and Table 3.8 respectively, in the Deform 3D

program, see Figure (3.23). The model curve was fitted once and saved in the material library, so as to use in all of the drilling operation simulations made with different parameters.

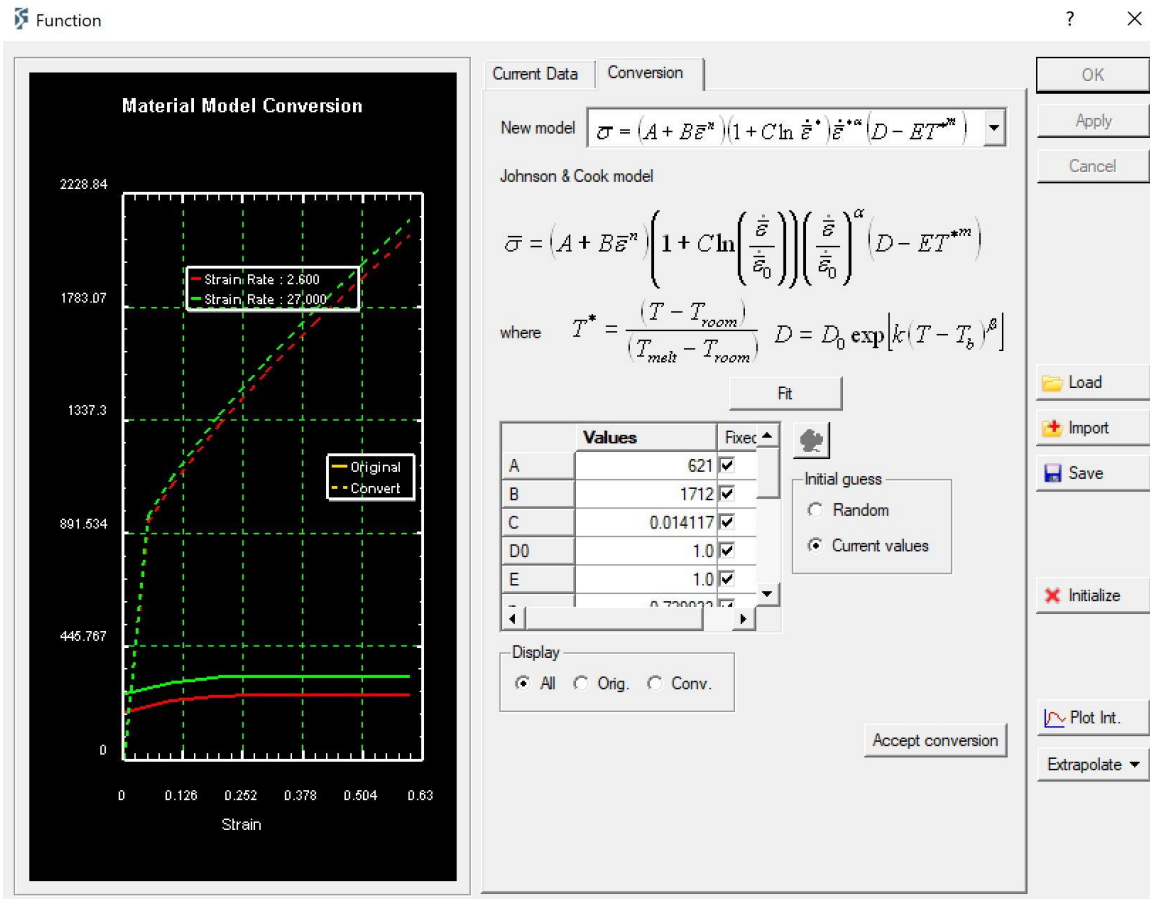


Figure 3.24. Johnson Cook model curve fitting in Deform 3D

The workpieces for both Inconel 718 and Incoloy A286 superalloys were modeled as plastic deformable with a mesh size of 80000 (eighty thousand). For the simulations, different mesh sizes were tried varying from 35 thousand to 135 thousand. However, not significant differences were observed in thrust force and torque results, but the lower mesh sizes led to bad chip geometry and the higher mesh sizes increased the run time and the result files occupied extremely large amount of hard disc space. So 80 thousand mesh size was used as a suitable mesh size for the simulations in terms of good chip geometry and reasonable run time. And the twist drills has been defined as a rigid body with a mesh size of 32000 (thirty two thousand). Table 3.9. shows mesh details of both workpiece and drill for drilling simulations of Incoloy A286 superalloy. Mesh details of twist drill used in drilling simulations of Inconel 718 superalloy was given in Chapter 3.1.2, Table 3.2. Moreover, geometrical inputs and simulation parameters are shown in Table 3.11,.

Table 3.9. Mesh details of workpieces for Inconel 718 and Incoloy A286 (above), Mesh details of drills for Incoloy A286 (below).

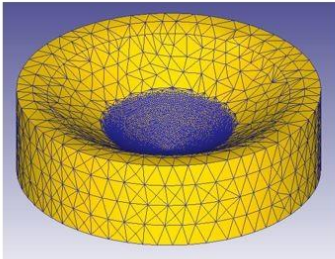
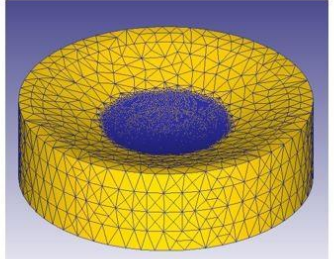
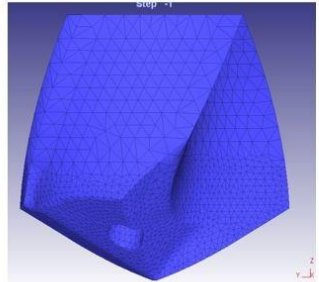
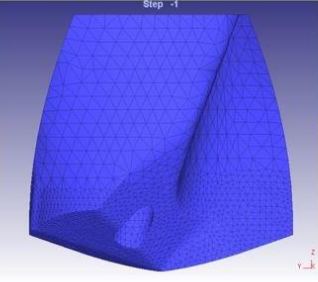
Workpiece (plastic)			
120	140	Mesh size	80000
		Mesh size ratio	10
		Mesh type	Tetrahedral
		No of elements	95143 102697
		No of nodes	20946 22433
Tool (Rigid)			
120	140	Mesh size	32000
		Mesh size ratio	4
		Mesh type	Tetrahedral
		No of elements	26851 6179
		No of nodes	45679 9311

Table 3.10. Geometrical inputs and simulation parameters for Incoloy A286

Main Category	Sub Category	Values
Cutting Parameters	Cutting Speed m/min	25, 50 m/min
	Feed Rate mm/rev	0.05, 0.1 mm/rev
	Temperature °C	20 °C
	Convection Coefficient	0.02 N/sec/mm/C
Tool-Workpiece Parameters	Shear Friction Factor	0.6
	Heat Transfer Coefficient	45 N/sec/mm/C
Drill Geometry Parameters	Drill bit Diameter	8.38 mm
	Number of Flutes (Cutting Edges)	2
	Helix Angle	28 Degrees
	Point Angle	120, 140 Degrees
Workpiece Geometry Parameters	Diameter	10 mm
	Thickness	3 mm
Simulation Steps	Number of Simulation Steps	2000 Steps
	Step Increment	10

The simulations were performed on two different computers, one having Core i7 processor with an 16 GB of RAM and the other having Core i5 processor with a 6 GB of RAM. The computation time on each computer for each simulation was approximately 35 to 40 hours to get the mean steady-state values of thrust forces and torques.

4. RESULTS AND DISCUSSION

4.1. Results

4.1.1. Simulation results

For each of the simulations, one complete revolution of the drill was sufficient to reach the steady state values for the thrust force and torque values. Therefore, the numerical result values belonging to steady state range of each simulation have been extracted and averaged to obtain a single mean numeric value. Typical numerical results and steady state region obtained in Deform 3D is shown in Figure 4.1. Past works show that, increasing elliptical translational motion due to drill vibrations, indicate a significant increase in the ranges of the torque and thrust, while maintaining essentially constant mean values, [53].

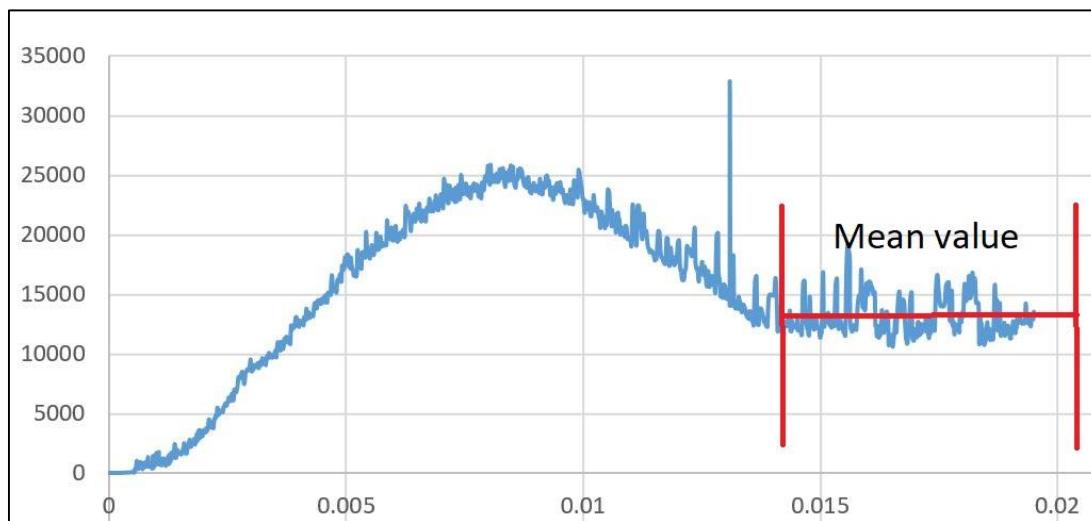


Figure 4.1. Typical simulation results, steady state region and the mean value in Deform 3D

The results of the drilling operation simulations of aged and annealed Inconel 718, are listed in Table 4.1.

Table 4.1. Simulation results for drilling Inconel 718

No. of operations	Cutting speed (m/min)	Feed rate (mm/rev)	Thrust force (N)		Torque (Nmm)	
			Aged	Annealed	Aged	Annealed
1	10	0.05	742.17	228.93	1888.21	660.61
2	10	0.1	816.49	294.01	3684.34	1395.78
3	20	0.05	599.78	219.75	1345.11	561.50
4	20	0.1	666.15	269.81	3280.43	1043.75

The results of drilling simulations of Incoloy A286 superalloy are listed in Table 4.2.

Table 4.2. Simulation results for drilling Incoloy A286

	No of Operations	Cutting speed m/min	Feed Rate mm/rev	Thrust Force (N)	Torque (Ncm)
Point angle 120	1	25	0.05	204.87	616.56
	2	50	0.05	190.77	574.52
	3	25	0.1	390.34	867.26
	4	50	0.1	233.54	847.57
Point angle 140	5	25	0.05	210.34	865.51
	6	50	0.05	198.78	637.25
	7	25	0.1	407.18	1273.33
	8	50	0.1	395.73	997.29

4.2. Discussion

In this section comparisons are made between the numerical results of torque and thrust force values with the numerical and experimental results in the literature.

As it is expected, numerical results show that torque and thrust force values increase with the increase of feed rate at constant cutting speed, in drilling simulations of aged and annealed Inconel 718 and Incoloy A286 superalloys, Figures (4.2, 4.3, 4.4 and 4.5). This can be explained by cutting mechanics theory; as the feed rate increases, instantaneous cutting area increases leading to larger cutting forces, thereby thrust force, and torque [37]. This result agrees with the experimental [10, 19, 49, 50, 51] and simulated results [10, 19, 50] found in the literature.

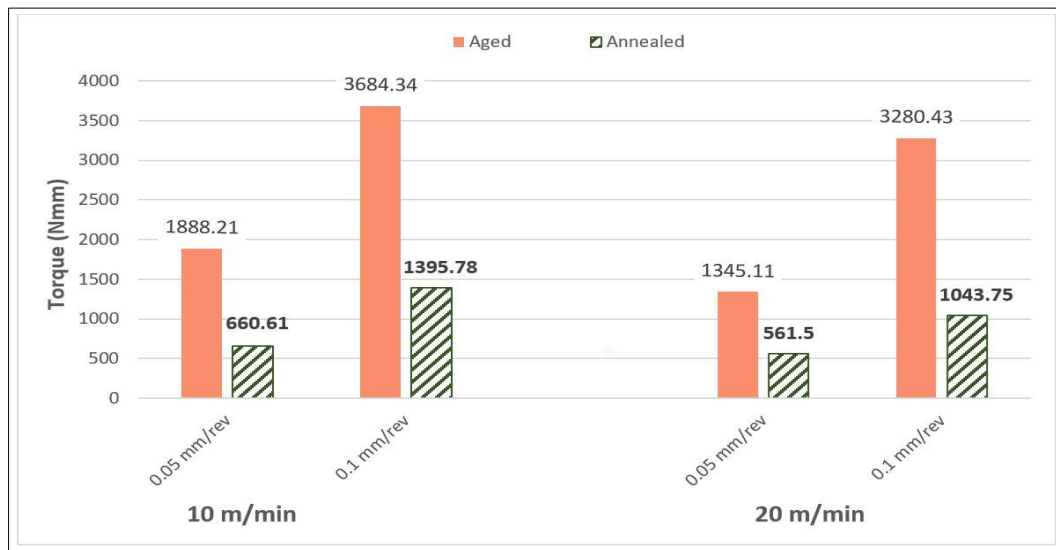


Figure 4.2. Increase of torques with increase of feed rate in drilling aged and annealed Inconel 718

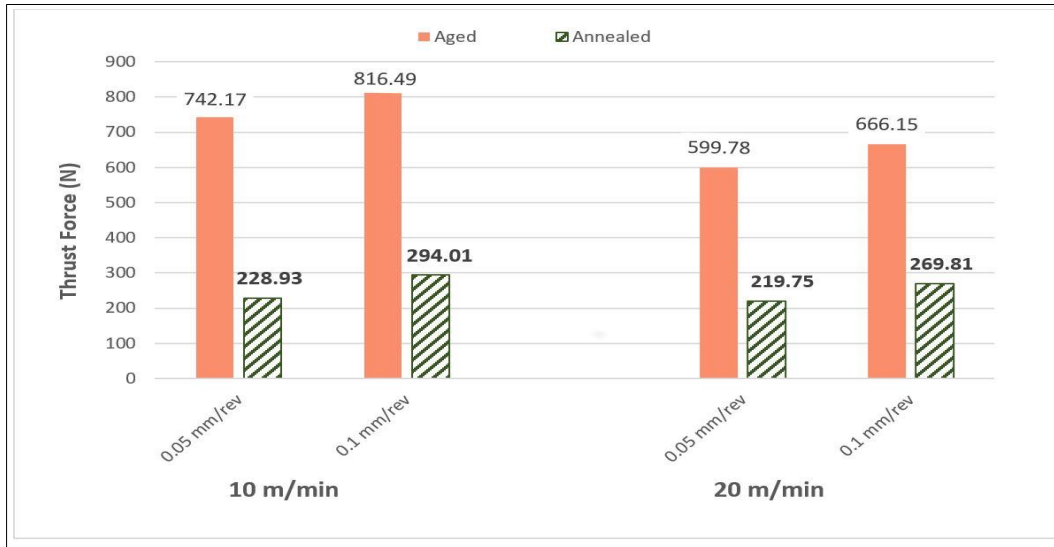


Figure 4.3. Increase of thrust forces with increase of feed rate in drilling aged and annealed Inconel 718

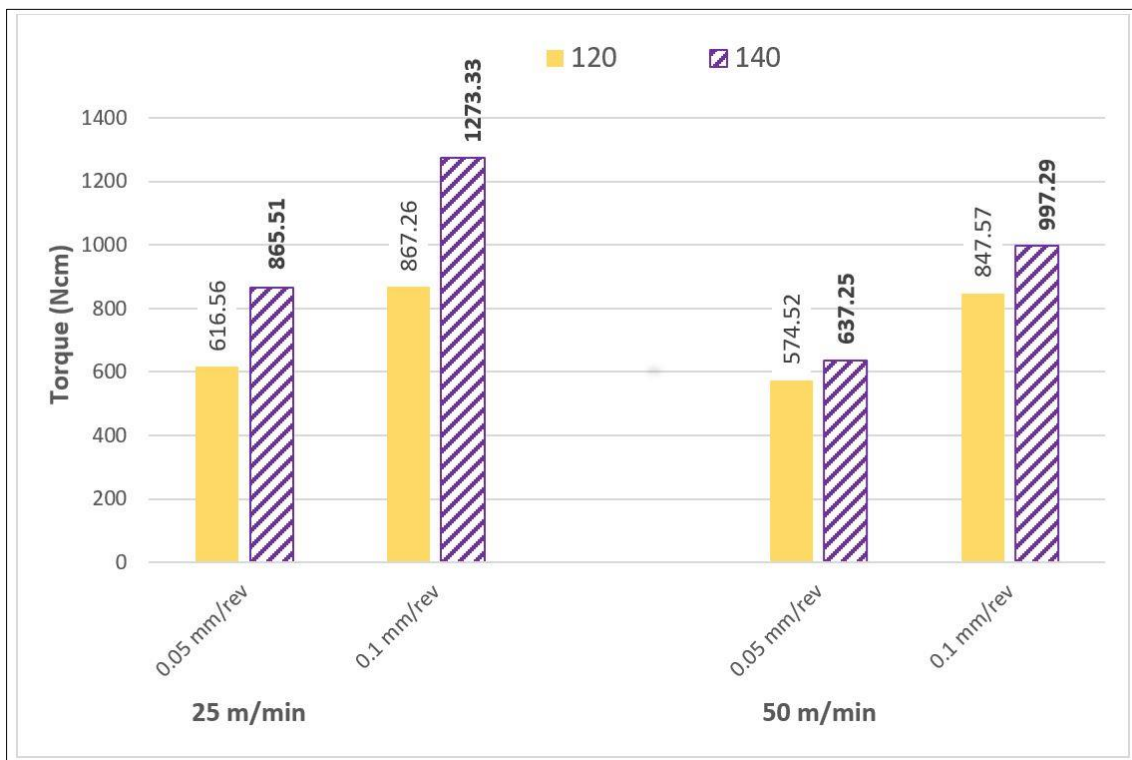


Figure 4.4. Increase of torques with increase of feed rate in drilling Incoloy A286

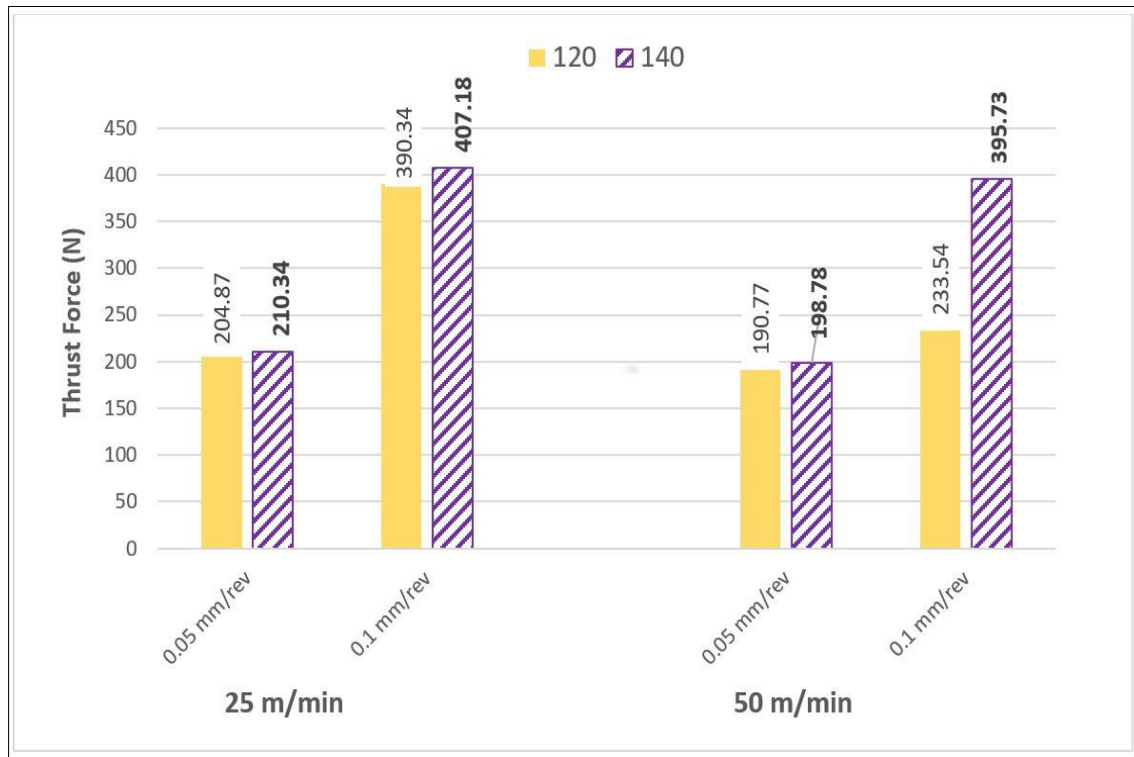


Figure 4.5. Increase of thrust forces with increase of feed rate in drilling Incoloy A286

The results also show that, the torque and thrust forces decrease with the increase of cutting speed at constant feed rate, Figures (4.6, 4.7, 4.8 and 4.9). This behaviour can be attributed to reduction of strength due to thermal softening effect within the considered cutting speed range for dry cutting conditions [38]. This result agrees with the experimental [19, 49, 51, 52] and simulated results [19] found in the literature.

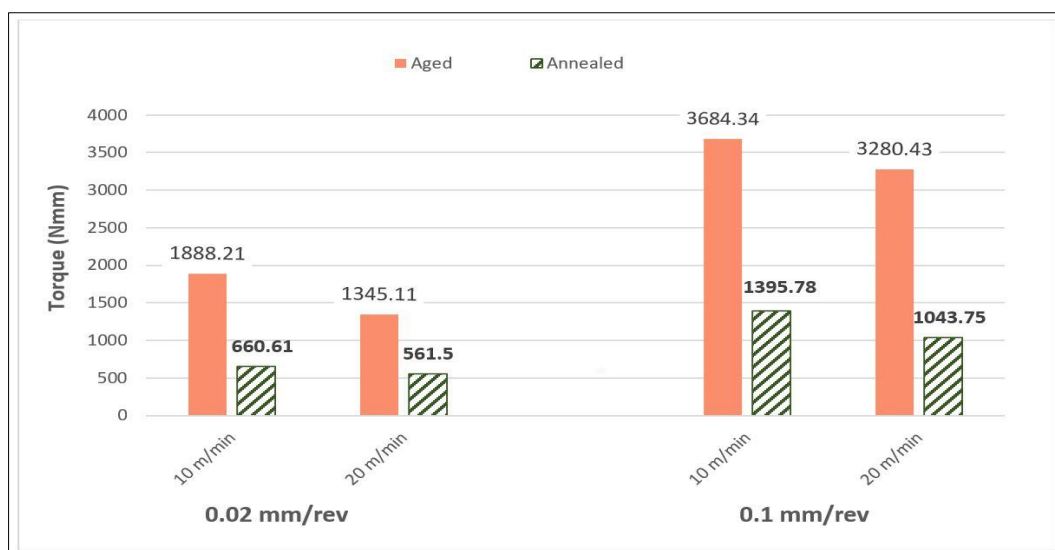


Figure 4.6. Decrease of torques with increase of cutting speed in drilling aged and annealed Inconel 718

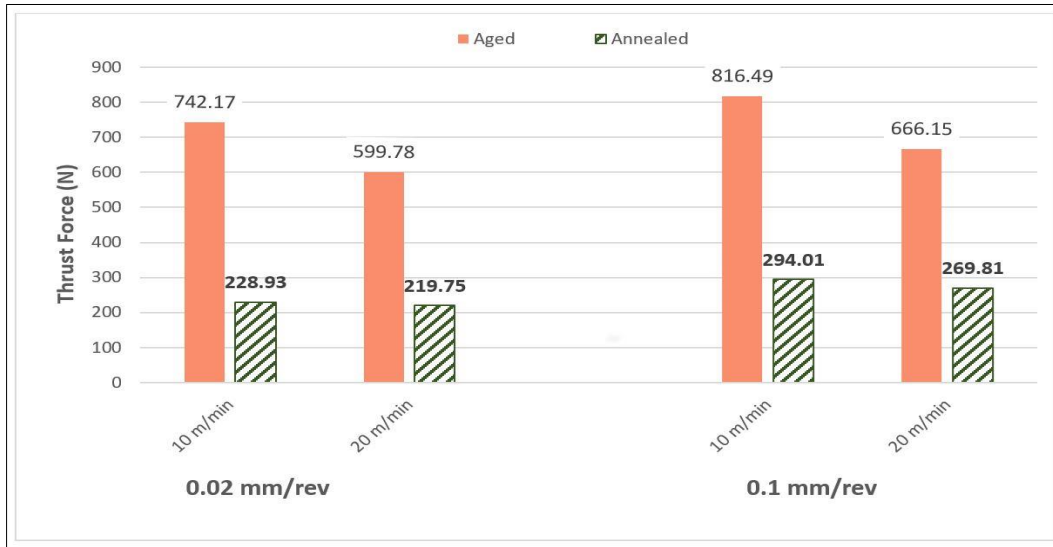


Figure 4.7. Decrease of thrust forces with increase of cutting speed in drilling aged and annealed Inconel 718

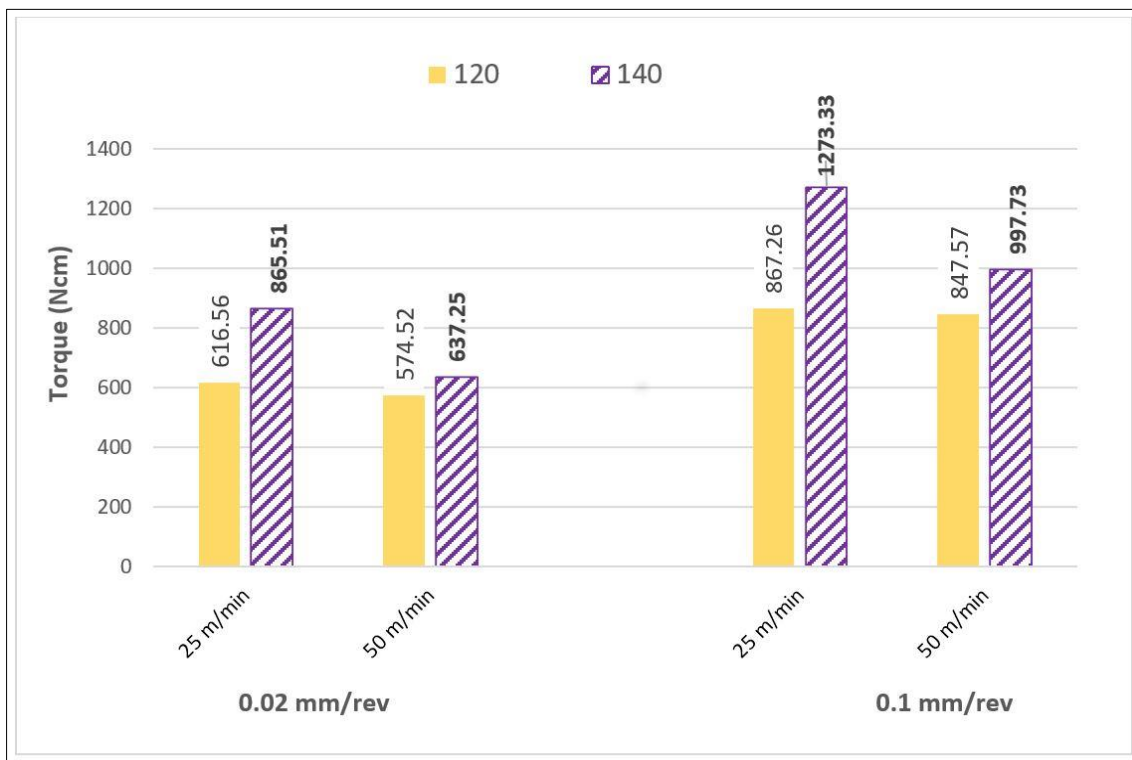


Figure 4.8. Decrease of torques with increase of cutting speed in drilling Incoloy A286

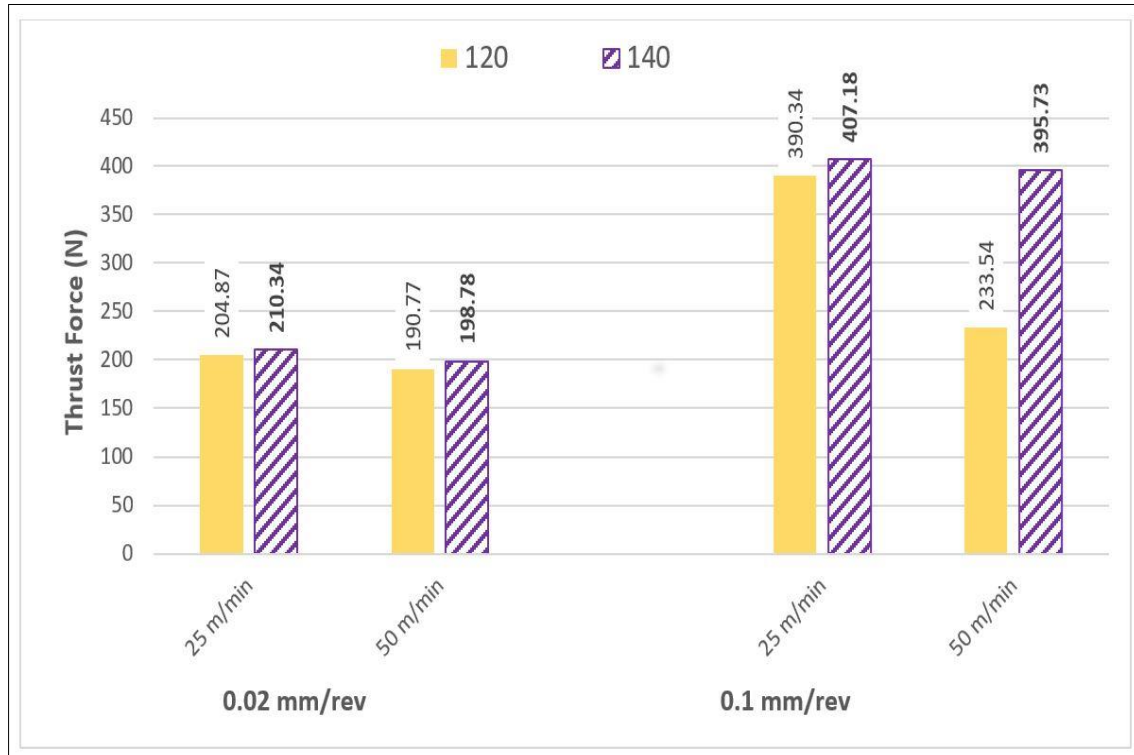


Figure 4.9. Decrease of thrust forces with increase of cutting speed in drilling Incoloy A286

In addition, for Incoloy A286, as can be seen from Figures (4.4, 4.5, 4.8 and 4.9), both the thrust force and torque values are higher for 140° point angle drill than 120° point angle drill for the same feed rate and cutting speed values, in all simulations.

It is worth noting here that, as it is known from the literature, the effects of cutting speed and drill point angle values on torque and thrust force may be complicated depending on the cutting speed range and point angle values studied, so the results here are valid for the ranges studied.

5. CONCLUSION AND FUTURE WORK

5.1. Conclusion

Summary of the present study:

In this study, drilling simulations of two types of Inconel 718 (aged and annealed) and Incoloy A286 superalloys have been modeled using Deform 3D software program. For drilling simulations of Inconel 718 superalloys, an uncoated carbide twist drill with a point angle of 140 degrees and for drilling Incoloy A286 superalloy, two carbide drills with point angles 120 and 140 degrees with TiN coating material were used. Two feed rates (0.05 and 0.1 mm/rev) were used for drilling simulations of all superalloys. But the cutting speeds were selected different; (10 and 20 m/min) for Inconel 718 superalloys, and (25 and 50 m/min) for Incoloy A286 superalloy were used. For the simulation operations, Johnson Cook material model was applied. The model parameters were obtained from the literature for Inconel 718 superalloys, but the J-C parameters for Incoloy A286 superalloy were determined in the scope of this thesis from tensile and Split Hopkins dynamic compression tests. Numerical studies are very important for checking the effectiveness of the software programs and predicting best cutting conditions in metal cutting operations, especially for drilling operations of hard to cut alloys. In this regard, the following conclusions can be drawn from the study;

- It is possible to predict cutting parameters for drilling superalloys using Deform 3D program.
- The thrust forces and drilling torques for three materials (aged and annealed Inconel 718 and Incoloy A286) increase with increasing feed rates and decrease with increasing cutting speeds.
- Generally, increase of cutting speed increased the cutting temperatures, thereby causing thermal softening of the material, and decreased thrust force and torque values.
- Thrust force and drilling torque values of aged Inconel 718 were remarkably larger than that of annealed Inconel 718, in all cases. This is already an expected trend because aged Inconel 718 has higher strength than does annealed Inconel 718 in plastic deformation.
- Cutting tool geometry plays important role on the cutting force values.

5.2. Future Work

Numerical study results show that, machinability of Inconel 718 and Incoloy A286 and effects of cutting parameters on cutting forces can be studied using Deform 3D. So the following suggestions can be evaluated for future work in drilling Inconel 718 and Incoloy A286;

- A wide range of cutting speeds and feed rates can be tried for predicting best cutting parameters.
- Different drill geometries and coating materials can be used and most suitable geometries can be predicted.
- Tool wear and surface roughness can be studied using the Deform 3D.
- Cryogenic drilling and wet drilling also can be studied and best conditions can be predicted.

REFERENCES

- [1] Groover, M. (2010). *Fundamentals of modern manufacturing materials, processes and systems* (5th ed.). NJ: John Wiley & Sons Inc.
- [2] Rivero, A. Aramendi, G., Herranz, S. and Lacalle, L. L. (2006). An experimental investigation of the effect of coatings and cutting parameters on the dry drilling performance of aluminium alloys. *Int J Adv Manuf Technol*, 28, 1-11.
- [3] Tonshoff, H. L., Spintig, W., König, W. and Neises, A. (1994). Machining of holes developments in drilling technology. *Annals of the CIRP*, 43(2), 551-560.
- [4] Ezugwu, E. O. (2005). Key improvements in the machining of difficult-to-cut aerospace superalloys. *International Journal of Machine Tools and Manufacture*, 45, 1353-1367.
- [5] Arrazola, P. J., Özel, T., Umbrello, D., Davies, M. and Jawahir, I. S. (2013). Recent advances in modelling of metal machining processes. *CIRP Annals - Manufacturing Technology*, 62, 695–718.
- [6] Naisson, P., Rech, J. and Paris, H. (2013). Analytical modeling of thrust force and torque in drilling. *Proceedings of the Institution of Mechanical Engineers, Part B: Journal of Engineering Manufacture*, 227(10), 1430-1441.
- [7] Karnik, S. R., Gaitonde, V. and Davim, J. P. (2007). Integrating Taguchi principle with genetic algorithm to minimize burr size in drilling of AISI 316L stainless steel using an artificial neural network model. *Proceedings of the Institution of Mechanical Engineers, Part B: Journal of Engineering Manufacture*, 221(12), 1695-1704.
- [8] Nouari, M., List, G., Girot, F. and Gehin, D. (2005). Effect of machining parameters and coating on wear mechanisms in dry drilling of aluminium alloys. *International Journal of Machine Tools and Manufacture*, 45(12), 1436-1442.
- [9] Motorcu, A., Kus, A. and Durgun, I. (2014). The evaluation of the effects of control factors on surface roughness in the drilling of Waspaloy superalloy. *Measurement*, 58, 394–408.
- [10] Nagaraj, M., Kumar, A., Ezilarasan, C. and Betala, R. (2019). Finite element modeling in drilling of Nimonic C-263 alloy using deform-3D. *Computer Modeling in Engineering & Sciences*, 118(3), 679-692.
- [11] Uçun, İ. (2016). 3D finite element modelling of drilling process of Al7075-T6 alloy and experimental validation. *Journal of Mechanical Science and Technology*, 30, 1843-1850.
- [12] Internet: A286 Data sheet, URL:
<https://www.upmet.com/sites/default/files/datasheets/a286>, Last visit on (02/10/2020).
- [13] Internet: A286 Data sheet, URL:
<https://www.upmet.com/sites/default/files/datasheets/a286>, Last visit on (02/10/2020).

- [14] Muraca, F. and Whittick, S. (1972). *Materials data handbook, stainless steel alloy A-286*. Huntsville, Alabama: Marshall Space Flight Center.
- [15] Grzesik, W. (2008). *Advanced machining processes of metallic materials* (1st ed.). Oxford: Elsevier.
- [16] Uçak, N., Çiçek, A., Oezkaya, E. and Aslantas, K. (2019). Finite element simulations of cutting force, torque, and temperature in drilling of Inconel 718. *Procedia CIRP*, 82, 47-52.
- [17] Beera, N., Özkaya, E. and Biermann, D. (2014). Drilling of Inconel 718 with geometry-modified twist drills. *Procedia CIRP*, 24, 49-55.
- [18] Attanasio, A., Fainia, F. and Outeiro, C. (2017). FEM simulation of tool wear in drilling. *Procedia CIRP*, 58, 440-444.
- [19] Parida, A. (2018). Simulation and experimental investigation of drilling of Ti-6Al-4V alloy. *International Journal of Lightweight Materials and Manufacture*, 1, 197-205.
- [20] Pawar, P., Ballav, R. and Kumar, A. (2017). Modeling and simulation of drilling process in Ti-6Al-4V, Al6061 using Deform-3D software. *International Journal of ChemTech Research*, 10(3), 137-142.
- [21] Díaz-Álvarez, J., Santiuste, C. and Miguélez, M. (2019). Experimental and numerical analysis of the influence of drill point angle when drilling biocomposites. *Composite Structures*, 209, 700-709.
- [22] Bagci, E. and Ozcelik, B. (2006). Finite element and experimental investigation of temperature changes on a twist drill in sequential dry drilling. *International Journal of Advanced Manufacturing Technology*, 28(7-8), 680-687.
- [23] Lin, W. S., Lee, B. Y. and Wu, C. L. (2001). Modeling the surface roughness and cutting force for turning. *Journal of Materials Processing Technology*, 108(3), 286-293.
- [24] Strenkowski, J. S., Hsieh, C. C. and Shih, A. J. (2004). An analytical finite element technique for predicting thrust force and torque in drilling. *International Journal of Machine Tools & Manufacture*, 44, 1413-1421.
- [25] Ucak, N. (2017). The effects of cutting conditions on cutting temperature and hole quality in drilling of inconel 718 using solid carbide drills. *Journal of Manufacturing Processes*, 31, 662-673.
- [26] Kivak, T. and Habalı, K. (2009). *Investigation of the effect of cutting parameters on surface roughness and chip formation in drilling of Inconel 718 super alloy*. 5th International Advanced Technology Symposium, Karabük, Turkey.
- [27] Şekerci, K. N., Duran, A., Şeker, U. and Yağmur, S. (2012). *Affects of cutting parameters of drilling AISI 316L material on cutting zone temperature*. 3rd National metal cutting Symposium, 5th October 2012, Ankara, Turkey.

- [28] Ozel, T., Llanos, I., Soriano, J. and Arrazola, P. J. (2011). 3D finite element modelling of chip formation process for machining inconel 718: Comparison of FE software predictions. *Machining science and technology journal: An International Journal*, 15(1), 21-46.
- [29] Gök, K., Türkes, E., Neseli, S., Saglam, H. and Gök, A. (2013). The validation as experimental and numerical of the values of thrust force and torque in drilling process. *Journal of Engineering Science and Technology Review*, 6(3), 93-99.
- [30] Bıyık, O. (2016). *Experimental investigation on the machinability of iron based superalloys*. Unpublished M.Sc. Thesis, Gazi University, Ankara.
- [31] Altintas, Y. (2012). *Manufacturing automation: Metal cutting mechanics, machine tool vibrations, and CNC design* (2nd ed.). New York: Cambridge University press.
- [32] Lee, J. and Chavez, C. L. (2018). Parameters affecting mechanical and thermal responses in bone drilling: A review. *Journal of Biomechanics*, 71, 4-21.
- [33] El-Hofy, G. And Abdel, H. (2013). *Fundamentals of machining processes: Conventional and nonconventional processes* (2nd ed.). New York: CRC Press.
- [34] Stephenson, D. A. and Agapiou, J. S. (2016). *Metal cutting theory and practice* (3rd ed.). New York: CRC Press.
- [35] Oezkaya, E. and Biermann, D. (2018). A new reverse engineering method to combine FEM and CFD simulation three-dimensional insight into the chipping zone during the drilling of Inconel 718 with internal cooling. *Machining Science and Technology*, 22(6), 881-898.
- [36] Johnson, G. R. and Cook, W. H. (1983). *A constitutive model and data for metals subjected to large strains, high strain rates and high temperatures*. Proceedings of the 7th Symposium on Ballistics, 541-547.
- [37] Wang, J. and Zhang, Q. (2008). A study of high-performance plane rake faced twist drills. Part I: Geometrical analysis and experimental investigation. *International Journal of Machine Tools & Manufacture*, 48, 1276-1285.
- [38] Sun, S., Brandt, M. and Dargusch, M. S. (2009). Characteristics of cutting forces and chip formation in machining of titanium alloys. *International Journal of Machine Tools & Manufacture*, 49, 561-568.
- [39] Davis, J. R. (2004). *Tensile testing* (Second Edition). Davis & Associates, 89-102.
- [40] Chen, W. and Song, B. (2011). *Split Hopkinson (Kolsky) bar design, testing and applications*. Springer Science, 28, 173-186.
- [41] Kaiser, M. A. (1998). *Advancements in the Split Hopkinson Bar*. Unpublished Master's Thesis, Virginia Polytechnic Institute, Virginia.
- [42] Kiranli, E. (2009). *Determination of material constitutive equation of a biomedical grade Ti6Al4V alloy for cross – wedge rolling*. Unpublished M.Sc Thesis, Izmir Institute of Technology, Izmir.

- [43] Tasneem, N. (2002). *Study of Wave Shaping Techniques of Split Hopkinson Pressure Bar Using Finite Element Analysis*. Unpublished Master's Thesis, Wichita State University, Wichita.
- [44] Internet: URL: <https://www.americanspecialmetals.com/inconelalloy718.html>, Last visit on (30.03.2020).
- [45] Internet: URL: <https://super-metals.com/wp-content/uploads/2015/03/Inconel-718.pdf>, Last visit, (30.03.2020).
- [46] Yegin, M. B. (2013). *High strain rate characterization of engineering materials*. Unpublished M.Sc. Thesis, Istanbul Technical University, Istanbul.
- [47] Lorentzon, J., Jarvstrat, N. and Josefson, B. L. (2009). Modelling of chip formation of alloy 718. *Journal of Materials Processing Technology*, 209, 4645-4653.
- [48] Uhlmann, E., Schulenburg, G. M. and Zettler, R. (2007). Finite element modeling and cutting simulation of Inconel 718. *Annals of the CIRP*, 56(1), 61-64.
- [49] Rahim, A. and Sasahara, E. H. (2009). Application of minimum quantity lubrication when drilling Nickel-based superalloy at high cutting speed. *Key Engineering Materials*, 407, 612-615.
- [50] Strenkowski, J. S., Hsieh, C. C. and Shih, A. J. (2004). An analytical finite element technique for predicting thrust force and torque in drilling. *International Journal of Machine Tools & Manufacture*, 44, 1413-1421.
- [51] Cuesta, M., Aristimuño, P., Garay, A. and Arrazola P. J. (2016). Heat transferred to the workpiece based on temperature measurements by IR technique in dry and lubricated drilling of Inconel 718. *Applied Thermal Engineering*, 104, 309-318.
- [52] Ema, S. (2012). Effects of twist drill point geometry on torque and thrust. *Sci. Rep. Fac. Educ. Gifu Univ. (Nat. Sci.)*, 36, 165-174.
- [53] Rincon, D. M., Ulsoy, A. G. and Kaftanoğlu, B. (1994). Effects of drill vibrations on cutting forces and torque. *CIRP annals*, 43(1), 59-62.

ATTACHMENTS

Attachment-1. Incoloy A-286 Material Certificate

江苏航太合金科技有限公司 Jiangsu Huntcc Alloys Technology Co., Ltd																							
产品质量证明书 MATERIAL CERTIFICATE																							
客户/ Customer Turkey Ankara						材料标准/ Material Standard: 技术协议成分参照 (API-6A718)																	
						合同号/ Contract No.: HT20140506																	
						证书编号/ Certificate NO.: HTH20140506																	
力学性能 (Mechanical Properties)																							
产品名称 Name:	规格尺寸 Spec.:	热处理批号 HT Lot No.:	炉号 Heat No.:	订单数量 PO. Qty	交货数量 Delivery Qty.	Tensile Test/ 拉伸试验			Impact Test/ 冲击试验			Hardness/ 硬度 (HRC)											
						Test Temp./ 试验温度 (°C)	Tensile strength/ 抗拉强度 (Mpa)	Yield strength/ 屈服强度 (Mpa)	Elon./ 延伸率 (%)	Red./ 断面收缩率 (%)	Dimension of Specimens/ 试样尺寸 10*10*55			1	2	3	4	5	6				
Incoloy A286	15*15*100(mm)	R201306-225	113-045	20	20	Normal	935	590	15														
化学成分 Chemical Composition%																							
炉号 Heat NO.	Ni	Cr	Mo	B	P	Al	Ti	C	Mn	Si	V	S	Fe	备注 Remark									
113-045	≤27	≤16	≤1.5	≤0.01	≤0.03	≤0.35	≤2.35	≤0.08	≤2.0	≤1.0	≤0.5	0.03	bal	/	/	/	/	/	/	/			
	25.22	14.79	1.28	0.003	0.014	0.18	2.28	0.05	1.11	0.02	0.19	0.02	bal	/	/	/	/	/	/	/			
项目/ ITEM												结果/ Result			证书编号/ Certificate No.								
UT												passed											
PT												passed											
RT																							
MT																							
VT																							
无损检测 NDT																							
We hereby certify the material herein has been manufactured/ tested and inspected in accordance with customer requirements and relate material standard. with satisfactory results.												推荐热处理 Heat Treatment											
我们在正证明这批材料控制制造、测试、检验完全符合客户和材料的标准要求。												固溶处理/Solution 时效处理/Age hardening											
												980°C, hold for 1 hours, cooling											
												720°C, hold for 16 hours, cool in air											
Inspected: Zhou												Check: Wang			Date: 2014-05-06			Stamp:					

Attachment-2. International standard of material Incoloy A286

DIN	EN
X6NiCrTiMoVB25-15-2	10302:2008

Attachment-3. Twist drill details used for drilling Incoloy A286

A30 0001 Series Walter Titex		Technical drawing
Standard	DIN 6537 K	<p>Technical drawing of a twist drill. The drawing shows a right-hand drill with a double-flute design. The diameter is $\phi 8.38$ and the length is 89 mm. The flute length is 47 mm, and the cutting edge length is 35 mm. The shank diameter is $\phi 10$ h6. The drill has a carbide tip and is made of A30 0001 Series Walter Titex material. The standard is DIN 6537 K. The cutting direction is right, the point angle is 120 and 140 degrees, there are 2 effective cutting edges, and there are 3 grinded faces.</p>
Material	Carbide	
Cutting direction	Right	
Point angle	120 and 140	
Effective cutting edges	2	
Grinded faces	3	



GAZİ GELECEKTİR..